Assessing the role of top-down techniques for improving regional estimates of artisanal and small-scale gold mining mercury emissions

by

Thandolwethu Dlamini

Submitted to the Technology and Policy Program
in partial fulfillment of the requirements for the degree of

Master of Science in Technology and Policy

at the

MASSACHUSETTS INSTITUTE OF TECHNOLOGY

September 2022

Author . . . . . .
Technology and Policy Program
August 05, 2022

Certified by . . . . . .
Noelle Selin
Professor, Institute for Data, Systems, and Society and Department of Earth, Atmospheric and Planetary Sciences
Director, Technology and Policy Program
Thesis Supervisor

Accepted by . . . . . .
Noelle Eckley Selin
Professor, Institute for Data, Systems, and Society and Department of Earth, Atmospheric and Planetary Sciences
Director, Technology and Policy Program

Assessing the role of top-down techniques for improving regional estimates of artisanal and small-scale gold mining mercury emissions

by

Thandolwethu Dlamini

Submitted to the Technology and Policy Program
on August 05, 2022, in partial fulfillment of the
requirements for the degree of
Master of Science in Technology and Policy

Abstract

ASGM is the world's largest source of anthropogenic Hg emissions and is common in Latin America, Sub-Saharan Africa, South Asia, and East Asia. However, the amount of mercury emitted from ASGM and contributing to global mercury emissions is subject to substantial uncertainty. Bottom-up studies have quantified sources of Hg, including ASGM, using data on underlying activities to estimate regional and global totals. In contrast, top-down studies have used atmospheric concentration measurements and models to constrain Hg emissions. However, no top-down estimates have yet been calculated for ASGM emissions. With GEOS-Chem's global-scale chemical transport model for Hg, we investigate whether and how ASGM-related Hg emissions can be quantified from existing regional measurement sites for gaseous elemental mercury (GEM). By combining our top-down method with existing bottom-up data, we improve estimates of Hg emissions from ASGM activities, using Peru and the Madre de Dios region of South America as case studies. We find that quantitative constraints on ASGM emissions are better provided by information on the shape of the probability distribution of GEM concentrations, such as the interquartile range and the 95% range, suggesting possible design guidelines for monitoring networks. The model-based analysis offers insights into improving regional estimates of ASGM emissions.

Thesis Supervisor: Noelle Selin
Title: Professor, Institute for Data, Systems, and Society and Department of Earth, Atmospheric and Planetary Sciences
Director, Technology and Policy Program

Acknowledgments

I am filled with sincere gratitude as I think about my time at MIT, the journey to get here and all the people that have helped me along the way. Most importantly, I would like to thank Noelle Selin, my research advisor, for welcoming me into her research group. This thesis would not have been possible without the Selin Group's training, challenging questions, and comradery. I am especially grateful to Aryeh Feinberg for his unyielding patience, for helping me with GEOS-Chem, and for encouragement. Thank you to all of the Selin Group's members. I have learned much from you.

I would like to thank Barb DeLaBarre, Elena Byrne, Ed Ballo, and Frank Field for all that they do for us. I am grateful to the TPPers in the classes ahead of us who provided invaluable advice on how to navigate MIT since we began our time remotely. Thanks to my TPP cohort (class of 22), we were able to learn, grow, and explore MIT in a supportive environment that we all created and sustained.

I am also grateful to everyone that has contributed to my academic journey so far. From my primary school teachers in Manzini, Eswatini to all the professors and I have had here at MIT, I am grateful. Thank you to my mentors that have provided guidance and support through out the years.

To Moreen: Thank you for your love that has kept me sane and helped me grow. You have been my strength through all the ups and downs of this journey. I love you.

And finally, thank you to my family in Eswatini. I would not be where I am today without your love and support. I love you.

This research was supported by a grant (#1924148) from the US National Science Foundation.

Contents

List of Figures

List of Tables

Chapter 1

Introduction

Mercury (Hg) is a severe health hazard in the environment and for people, especially fetuses and young children[1]. The release of mercury into the atmosphere results from human activities and natural processes. Upon release, mercury moves between the air, soils, and waters until, eventually, it is removed from the system through burial in coastal and deep ocean sediments, lake sediments, and subsurface soils [2]. Moreover, mercury can travel great distances when emitted into the atmosphere, contaminating ecosystems, fish, birds, mammals, and human food chains [2]. Recent estimates, as seen in Figure 1-1, indicate that about 38% of global Hg emissions come from ASGM, making it the largest source of Hg pollution to the atmosphere and hydrosphere around the world[3]. However, the amount of Hg released by ASGM activities and the extent to which it is transported regionally and globally is highly uncertain. This thesis examines how top-down emissions estimation techniques can help reduce the uncertainty in ASGM Hg estimates. First, we will briefly describe the Hg problem in ASGM. As a next step, we review the state of atmospheric Hg monitoring and modeling in regions where ASGM activities are prevalent. In addition, we use observed atmospheric Hg concentrations and atmospheric Hg predictions produced by the GEOS-Chem Model to come up with the first-ever top-down estimates of ASGM Hg emissions for a region in Peru. Lastly, we synthesize the findings and make recommendations for policymakers to use monitoring and modeling to better understand ASGM Hg emissions. To comply with the Minamata Convention, we will use the term "Hg emissions" throughout this thesis to refer to Hg discharges into the atmosphere and "Hg releases" to refer to Hg discharges into the ground and water. "Hg discharge" will be used when referring to both emissions and releases.

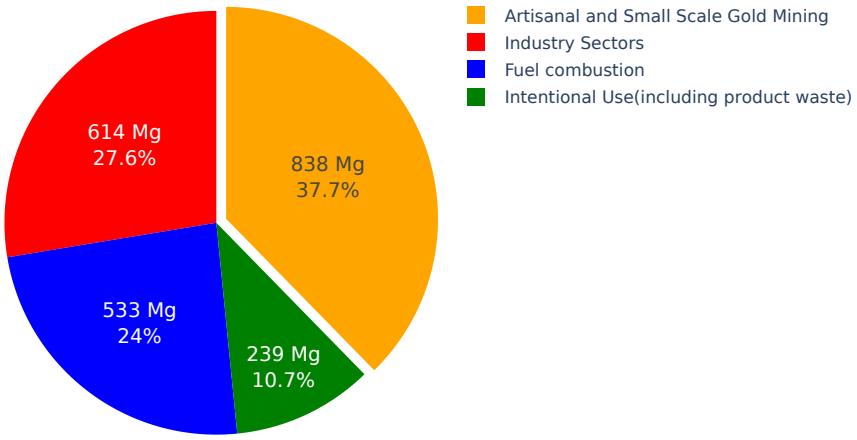

Figure 1-1: Pie chart showing the 2018 global mercury assessment (GMA 2018) ASGM Hg emission estimates for different sectors. ASGM is estimated to emit the most Hg emissions (shown in orange) at 838 Mg, followed by industry sectors (shown in red) at 614 Mg, then fuel combustion (shown in blue) at 533 Mg, and finally, intentional use sectors excluding ASGM (show in green) at 239 Mg [3].

1.1 Motivation

More than 100 million people depend on artisanal and small-scale gold mining (ASGM) for their livelihood globally, particularly in the over 81 countries, predominantly in the global south where ASGM exists[4]. Additionally, ASGM is an essential source of income and an opportunity for rural development in countries where options and alternatives to ASGM for generating income to buy necessities of daily life are in short supply or nonexistent [4]. It is estimated that around 10 to 20 million (ASGM) miners are employed in ASGM worldwide - about a third of them are women - and they provide 90% of the global gold mining workforce and extract about 20% of the world's gold annually [4]. For example, in Peru, ASGM sustains the livelihoods of an estimated 1 million people, and between 300,000 and 500,000 miners were involved in Peru's ASGM sector as of 2014. Despite being a vital source of livelihood for the communities that practice ASGM, its activities often lead to several environmental, human, and social harms. In addition to Hg releases to the environment, ASGM externalities include deforestation, tropical

diseases such as malaria, dangerous and unsafe working conditions, crime and exploitation of indigenous communities, diesel and gasoline spills, and human trafficking [5].

While most of the Hg pollution from ASGM is local, its ability to travel across borders and contaminate distant ecosystems bolsters the case for concerted global efforts to eliminate Hg pollution in all forms, including ASGM Hg pollution. The Minamata Convention (MC) is one of the unified global efforts to combat Hg pollution. It is a legally binding global treaty with 137 parties as of this writing, and its goal is to protect human health and the environment from the adverse effects of mercury. The MC's text comprises articles that address different sources of Hg pollution, including ASGM Hg emissions[6]. This thesis work is inspired by the need to improve our understanding of Hg emissions and Hg's regional and global transport to ensure that policies and actions taken to reduce ASGM Hg emissions are informed by the best available science and take advantage of all resources at our disposal to create actionable scientific knowledge.

1.2 Mercury Use in Artisanal and Small-Scale Gold Mining

During ASGM, Hg is added to the gold ore to form a mercury-gold amalgam, a mixture of about equal amounts of Hg and gold[7]. Heat is applied to the amalgam, which evaporates the Hg, leaving the gold behind. Gold extraction using this method is popular with the ASGM community since it is inexpensive, easy to use, and quick [7]. Moreover, Hg is relatively effective at capturing gold when there are no alternatives but often captures less than 40% [8]. There is usually a tremendous amount of Hg vapor in the air around amalgam burning sites, much higher than the World Health Organization(WHO) limit of 1.0 $\mu g/m^3$[1]. The Hg emissions in ASGM are harmful to miners and members of their communities. Additionally, humans and ecosystems far away are also exposed to Hg risks because Hg travels globally through the atmosphere. As volatilized Hg subsequently settles in soil, rivers, bays, and oceans, anaerobic organisms transform it into methylmercury, and water bodies can become contaminated with methylmercury[3]. Methylmercury is absorbed and ingested by phytoplankton, zooplankton, and fish, and predator species such as sharks and swordfish that live a long time accumulate methylmercury and can cause health damages to people who eat fish[1].

1.3 ASGM Measures in the Minamata Convention

The MC was agreed upon at the fifth meeting of the Intergovernmental Negotiating Committee on Hg in Geneva, Switzerland, in January 2013 and formally adopted in October that year in Kumamoto, Japan. Moreover, the treaty entered into force on 16 August 2017, 90 days after the 50^{th} instrument of ratification was deposited, and currently has 137 parties to the convention[6]. The MC's goal is to protect human health and the environment from the adverse effects of mercury, and it affirmed that global action is essential to address the Hg pollution problem. Article 7 and Annex C of the MC target ASGM. Article 7 requires countries where Hg use in ASGM is "more than insignificant" to develop a National Action Plan (NAP) that details ways to reduce and, where possible, eliminate the use of Hg and Hg compounds. Each country should include in its NAP actions to stop some of the worst practices of ASGM, which include, among other things, (i) whole ore amalgamation, (ii) open burning of amalgam, (iii) burning of amalgam in residential areas (iv), and cyanide leaching in sediment or tailings to which Hg has been added without first removing the Hg [3]. Moreover, countries are required to include in their NAPs baseline estimates the quantities of Hg used in ASGM. The UNEP *Guidance Document: Developing a National Action Plan to Reduce and, Where Feasible, Eliminate Mercury Use in Artisanal and Small-Scale Gold Mining*(MC Monitoring Guidance) [9] states that the goal should be to produce an estimate with an accuracy of $\pm$ 30% and, at worst, $\pm$ 50%. This is argued to be an obtainable level of confidence in the context of effort, time, and financial resources while being good enough to inform the NAP and allow for prioritization of actions [9]. A vital component of the MC is Article 22, which specifies a variety of information that must be included when conducting the effectiveness evaluation of the MC. The article states that "the Conference of the Parties shall, at its first meeting, initiate the establishment of arrangements for providing itself with comparable monitoring data on the presence and movement of Hg and Hg compounds in the environment as well as trends in levels of Hg and Hg compounds observed in biotic media and vulnerable populations." This thesis aims to demonstrate the value atmospheric modeling and monitoring would add to the process mandated by article 22 by evaluating the state of atmospheric monitoring and modeling in world regions with high ASGM incidence. Moreover, the role and the value of monitoring and modeling in the effectiveness evaluation of the MC were emphasized in the recently published MC Monitoring Guidance[10].

1.4 Case Study Region

The estimated amounts of ASGM Hg emissions from the different countries vary. This is illustrated in Figure 1-2, which is a map showing the GMA 2018 ASGM Hg^0 emission estimates for 2015 for all countries worldwide that have ASGM Hg^0 emissions and a bar chart showing countries estimated to emit more than 10 tons/year of Hg from ASGM [3]. Moreover, the GMA 2018 reported that ASGM Hg emissions in Latin America were the highest [3]. Figure 1-2 shows that Latin America has the highest concentration of countries have estimated ASGM Hg emissions above 40 tons/year [3]. Furthermore, Latin America has the highest average ratio of mercury losses to gold production at 4.63, according to Yoshimura et al.'s[11] estimate. This means that for every gram of gold produced, 4.63 grams of Hg are "lost" (i.e. discharged to the environment). Africa and Asia have the lowest at 1.96 and 1.23, respectively. However, atmospheric Hg data from Latin America are rare; hence Hg dynamics in the region are not well understood.

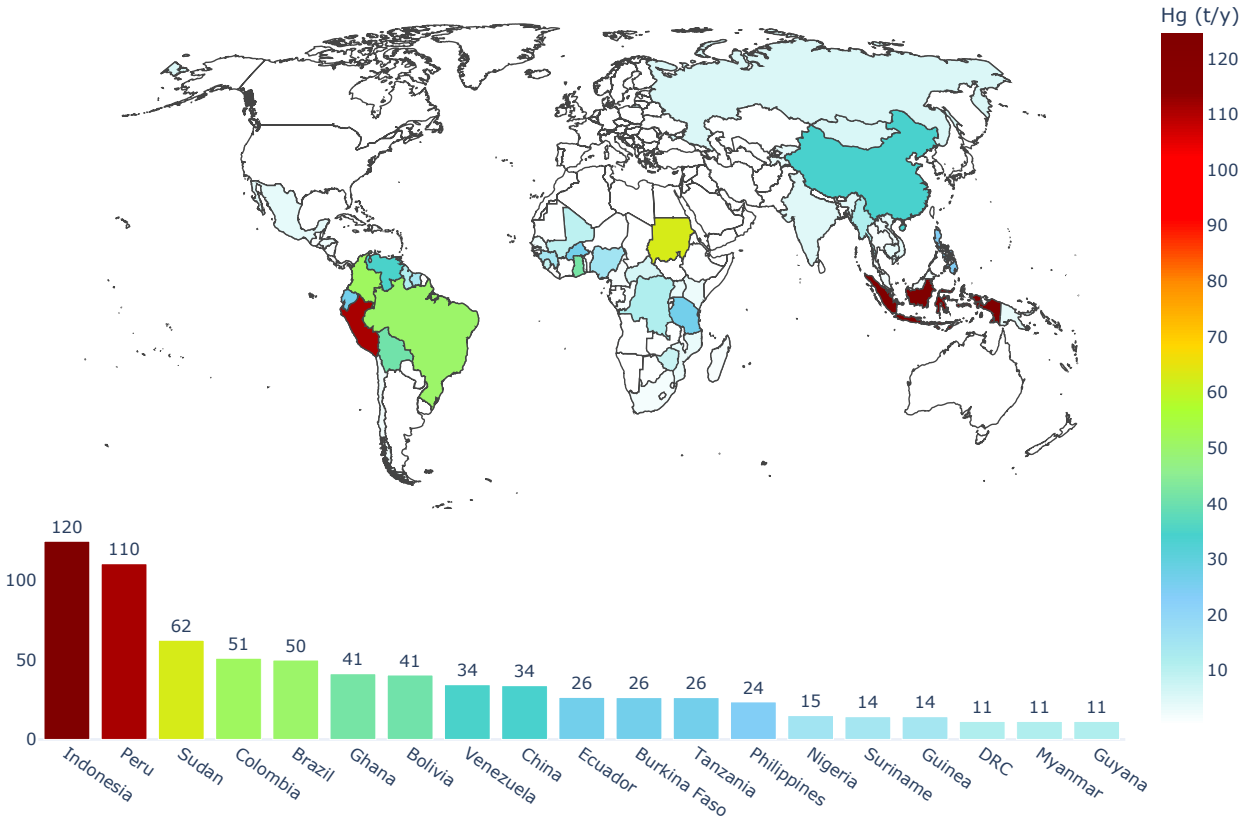

Figure 1-2: World map showing the GMA 2018 ASGM Hg^0 emission estimates for all countries worldwide that have estimated ASGM Hg^0 emissions and a bar chart showing the countries estimated to emit more than 10 tons/year of Hg from ASGM [3].

Peru is the source of the largest ASGM Hg emissions in Latin America and the second largest source globally, as seen in Figure 1-2. In Peru, the Madre de Dios region provides an ideal place for Hg research because the process of ASGM in this region involves mainly an amalgamation of the whole ore, which is the more Hg-intensive of all ASGM processes and is recommended as a "worst practice" to be eliminated by the Minamata Convention[12]. The process of whole ore amalgamation involves pouring liquid Hg into old oil drums and mixing it with gold-flecked sediment. Miners spend hours immersed in toxic mud with their pants rolled up to their knees in traditional winemaking style. The ratio of liquid Hg to gold amalgam is around 2:1[13, 14, 15]. As soon as the mercury amalgam is formed, miners burn it off to sell the gold. Hg is often burned off by "gold-changers" in the open air with blowtorches in market areas also occupied by other local small businesses. In addition to posing environmental risks, this mercury can also harm women and children[16].

The Madre de Dios region is estimated to be the source of the largest quantities of Hg to the environment and the atmosphere[17]. Madre de Dios, shown by the red outline in Figure 1-3, is a rainforest region between Bolivia and Brazil and covers roughly 85,000 square kilometers. The region's name is derived from the name of a major river that runs through it, and smaller streams and rivers cross through it to provide transportation and fishing for indigenous communities. Furthermore, these waterways are the main sites of ASGM and, subsequently, Hg contamination [18, 17]. The other regions around Madre de Dios that are sources of large quantities of Hg are outlined in Figure 1-3. The department of Puno is highlighted in purple, Arequipa is shown by the blue outline, Ayachucho with the green outline, Apurimac with the orange outline, and Cusco with the maroon outline.

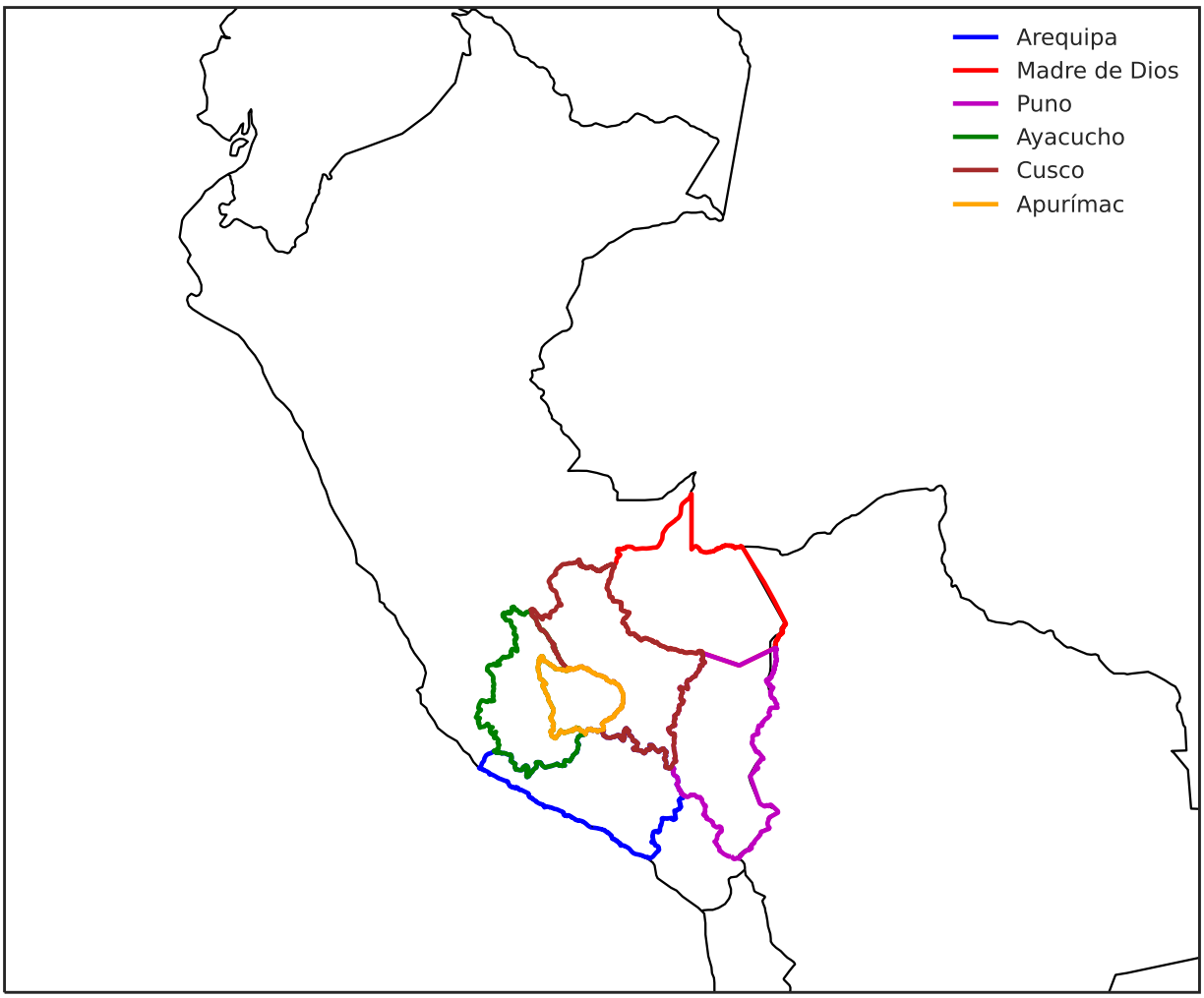

Figure 1-3: Peruvian departments studied in this thesis. Some of these departments were predicted to be the prominent sources of ASGM Hg releases according to the Artisanal Gold Council's Inventory Report for the ASGM sector in Peru (2017)[17].

Environmental and human health effects of ASGM Hg pollution have been extensively studied in Madre de Dios. This thesis project seeks to complement previous studies and distinguish itself by investigating the extent to which the GEOS-Chem model can leverage existing measurements of Hg in the atmosphere to produce top-down estimates of ASGM Hg emissions from Madre de Dios and surrounding departments with reported ASGM activities.

1.5 Thesis Questions

Several studies have identified atmospheric mercury monitoring as a primary and appropriate method to assess the effectiveness of the MC [19, 20, 21, 3]. Additionally, according to the MC's

Monitoring Guidance one of the primary objectives of monitoring Hg in the atmosphere is to provide data for the development and improvement of transport and chemistry models[10]. However, few studies have shown how monitoring data and atmospheric models can inform policy on ASGM Hg emissions. Therefore, we seek to answer the following questions based on the assumption that using chemical transport models (CTMs), such as GEOS-Chem, we can synthesize data from national and global Hg inventories and atmospheric monitoring networks for tracking progress and assessing MC's effectiveness:

1. To what extent can regional atmospheric modeling and monitoring help reconcile the differences in the current global estimates of emissions and national emissions?

2. How can regional monitoring networks improve the utility of models for evaluating the effectiveness of MCs?

3. Which atmospheric modeling and monitoring should be prioritized by governments and policy makers to obtain actionable information about Hg reductions?

1.6 Organization

This introductory chapter has provided a general background on ASGM concerning Hg emissions and the extent of global efforts to protect people and the environment from the adverse effects of Hg pollution. Chapter 2 compares the temporal and spatial characteristics of observed and modeled atmospheric Hg concentrations. It addresses aspects of the first thesis question by evaluating GEOS-Chem modeled atmospheric Hg concentrations across Latin America with observed Hg concentrations at various regional sites. In chapter 3, a method is presented for estimating ASGM Hg emissions. Using atmospheric modeling and monitoring, it is demonstrated how different ASGM Hg emissions inventories can be reconciled and how monitoring networks can enhance models' utility. Finally, chapter 4 presents policy recommendations and conclusions to address the third research question.

Chapter 2

Use of a Global Model to Understand Atmospheric Mercury Observations at Monitoring Sites in Latin America

Environmental pollution from Hg damages ecosystems through Hg's transformation into toxic methylmercury and bio-accumulation in food chains. Further, Hg is highly mobile in the atmosphere, allowing it to travel to faraway places, resulting in worldwide distribution of its elemental form, Hg^0 , which can last for as long as six months in the atmosphere[22, 23]. Hg in the atmosphere can be classified as gaseous elemental Hg (GEM), gaseous oxidized Hg (GOM), and particulate-bound Hg (PBM) [24, 25, 26]. In most cases, Hg emissions occur as gaseous elemental Hg^0 , which is relatively inert and sparingly soluble in water [22]. Since most Hg entering ecosystems comes from the atmosphere, monitoring and modeling atmospheric Hg and Hg deposition enables us to understand its biogeochemical cycle. In addition, a better understanding of Hg's circulation in the environment would enable effective policies to reduce its harmful effects.

In this chapter, we compare the outputs of the GEOS-Chem model with observed Hg at multiple sites in Latin America from two monitoring networks. We combine simulations of Hg in the atmosphere produced by the GEOS-Chem CTM (Sect. 2.2.2 - Sect. 2.2.2) with ground-based observations of atmospheric total gaseous mercury (TGM) (Sect. 2.2.3) from the Global Mercury Observation System (GMOS)[19] and gaseous elemental mercury (GEM) data from a network of passive air samplers (PAS)[27] distributed across Latin America. Then, we present comparisons

between observations and model outputs and discuss the implications of the current state of atmospheric monitoring and modeling atmospheric Hg in Latin America(Sect. 2.3). Finally, we summarize conclusions from the analysis (Sect. 2.4).

2.1 Background

Hg monitoring networks and atmospheric Hg models are closely interconnected in the literature. For instance, Gustin et al's.[28] describe up-to-date scientific thinking regarding mercury in the environment, monitoring and modeling techniques, and how they relate to Minamata Convention on Mercury. Notably, the mutual dependency between atmospheric modeling and monitoring is presented in the MC's "Monitoring Guidance Document"[10], which states that observations are needed not only to detect and quantify changes but also to improve and evaluate models of mercury transport, fate, exposure, and impacts[10]. Similarly, Sprovieri et al.[19] emphasize the importance of consistent global Hg measurements to validate regional and global-scale models. According to Brasseur and Jacob[29], it is crucial to have a large ensemble of observations to evaluate atmospheric modeling outputs.

Data from passive and active sampling sites are evaluated in this thesis. The MC's "Monitoring Guidance Document"[10] provides a comprehensive definition and comparison of active and passive air sampling. Active air samplers, particularly automated ones, can deliver high-frequency data in a short period from as little as 5 seconds to 5 minutes[10]. However, they may be complex and costly to set up and operate. In contrast to active samplers, PAS are low-cost, inexpensive, and do not require electricity, moving parts, pump operation, or calibration[30]. Despite their small size, they can be deployed at background, remote, urban, and hotspot sites without worrying about media failures[10].

Some world regions, such as Latin America and Africa, with high ASGM Hg emissions, have not been subject to detailed model-observation comparisons. This may be attributed to these regions' lack of wide coverage of required high-frequency atmospheric Hg monitoring capacity, as shown in Figure 2-1, which illustrates the distribution of different Hg monitoring networks worldwide[3]. It is evident in Figure 2-1 that Latin America, Africa, and South East Asia remain

significantly behind Europe and North America regarding access to large observation ensembles. A majority of the sampling sites present in these regions are PASs.

Figure 2-1: Global map of Hg monitoring networks [3]

2.2 Methods

2.2.1 GEOS-Chem Description

The global atmospheric Hg concentration was simulated using version 12.8.1 of GEOS-Chem, whose Hg simulation is described by Horowitz et al.[22]. All the simulations in this study were run globally for 47 vertical layers at a resolution of 2.0×2.5, which is approximately equal to a

222 km×277.5 km grid square at the equator [22]. Moreover, the MERRA-2 assimilated meteorological data [31] drive the model's atmospheric transport, which calculates atmospheric Hg from three tracers: elemental Hg, Hg^0, divalent Hg, Hg^{2+}, and particulate-bound divalent Hg, Hg^p. The Hg chemical scheme in the GEOS-Chem version used in this study considers bromine (Br) to be the primary Hg^0 oxidant[22] and employs monthly mean Br oxidant concentrations from Schmidt et al.[32].

2.2.2 GEOS-Chem Simulations

The GMA 2018 emissions inventory was used to represent anthropogenic emissions sources from all sectors[33]. Different inputs to the GEOS-Chem model, such as emissions sources, can be toggled on or off depending on the research objective; hence a reference simulation, Base (ASGM = ON) simulation was created by turning on all Hg emissions sources globally. Moreover, a No ASGM (ASGM = OFF) simulation was generated by turning off the ASGM source globally to evaluate the contribution of ASGM to the baseline modeled Hg^0 in the atmosphere by calculating the difference between the Base (ASGM = ON) simulation and No ASGM (ASGM = OFF) simulation . Table 2.1 describes the simulations that were conducted in detail.

Table 2.1: GEOS-Chem simulations conducted

Simulation Name	Period	Resolution	Description
Base (ASGM=ON)	2010-2016	2.0×2.5	All Hg anthropogenic emission sources are turned on
No ASGM (ASGM=OFF)	2010-2016	2.0×2.5	All ASGM emissions are turned off

The simulation frequency was set to output daily Hg^0 averages at the global scale, while the Hg^0 output for the grid boxes corresponding to the locations of the GMOS observation sites was set to an hourly frequency. The GEOS-Chem outputs for all the simulations were in units of parts per trillion (ppt) and were converted to ngm^{-3} at standard temperature and pressure (273 K, 1 atm) to compare them to observations.

2.2.3 Atmospheric Mercury Monitoring Sites in Latin America

The GMOS network is one of a few major projects to develop a global observing system for Hg pollution. GMOS aims to provide high-quality Hg data sets in the Northern and Southern

hemispheres to enable a more comprehensive assessment of atmospheric Hg concentrations and their dependence on meteorology, long-range atmospheric transport, and atmospheric emissions[19]. A vast network of ground-based monitoring stations, regular oceanographic cruises, and lower, upper, and stratospheric measurements make up this European Union-funded project [34, 19]. More than 40 ground-based monitoring sites constitute the GMOS network, covering many regions with limited to no observational data before GMOS[19]. The GMOS monitoring network has five sites in Latin America that actively monitor Hg levels. A detailed analysis of the Sisal, Calhau, Manaus, Nieuw Nickerie, and Bariloche sites was conducted by Sprovieri et al.[19], and the Chalcataya site was analyzed in detail by Koenig et al.[34]. A summary of the sites' characteristics is shown in Table 2.2. Moreover, the distribution of these GMOS sites in Latin America is indicated by the red triangles in Figure 2-2, which is a map showing the names and locations of the GMOS Monitoring Network Sites and Passive Sampler sites in Latin America [27, 34]. Moreover, PAS data from the Latin American Passive Air sampling Network (LAPAN), which was analyzed in detail by Quant et al.[27], was used for the model observation comparison. The respective locations of the PAS sites are shown by the blue circles in Figure 2-2.

Table 2.2: Characteristics of the GMOS sites evaluated [34, 19].

Site	Site abbrev	Latitude	Longitude	Physical Setting	Elevation (m)	Number of Records (days)	Site Type	Measurement Period
Sisal, Mexico	SIS	21.16	-90.05	Coastal site	7	320	Secondary	1/1/2010-1/1/2016
Calhau, Cape Verde	CAL	16.86	-24.87	Coastal site	10	309	Secondary	1/1/2013-12/1/2014
Nieuw Nickerie, Suriname	NIK	5.93	-56.98	Coastal site	1	215	Secondary	3/1/2007-12/1/2014
Manaus, Brazil	MAN	-2.89	-59.96	Amazon site	110	100	Master	1/1/2013-12/1/2014
Chalcataya, Bolivia	CHC	-16.2	-68.12	Mountain site	5340	333	Secondary	7/1/2014-2/1/2016
Bariloche, Agentina	BAR	-41.13	-72.42	Mountain site	800	333	Master	10/1/2012-7/1/2017

The GMOS sites are classified as either secondary or master sites in Table2.2 to indicate the type of data collected and the type of equipment used at the site. Master stations are those where Gaseous Elemental Hg (GEM, i.e., the gas phase Hg in its ground electronic state), Gaseous Oxidized Hg (GOM, i.e., the oxidized gas phase Hg compounds), Hg associated with suspended particulate matter (PBM2.5) and Hg in precipitation are continuously measured while secondary stations are those where only GEM and Hg in precipitation are continuously measured [19, 21, 34].

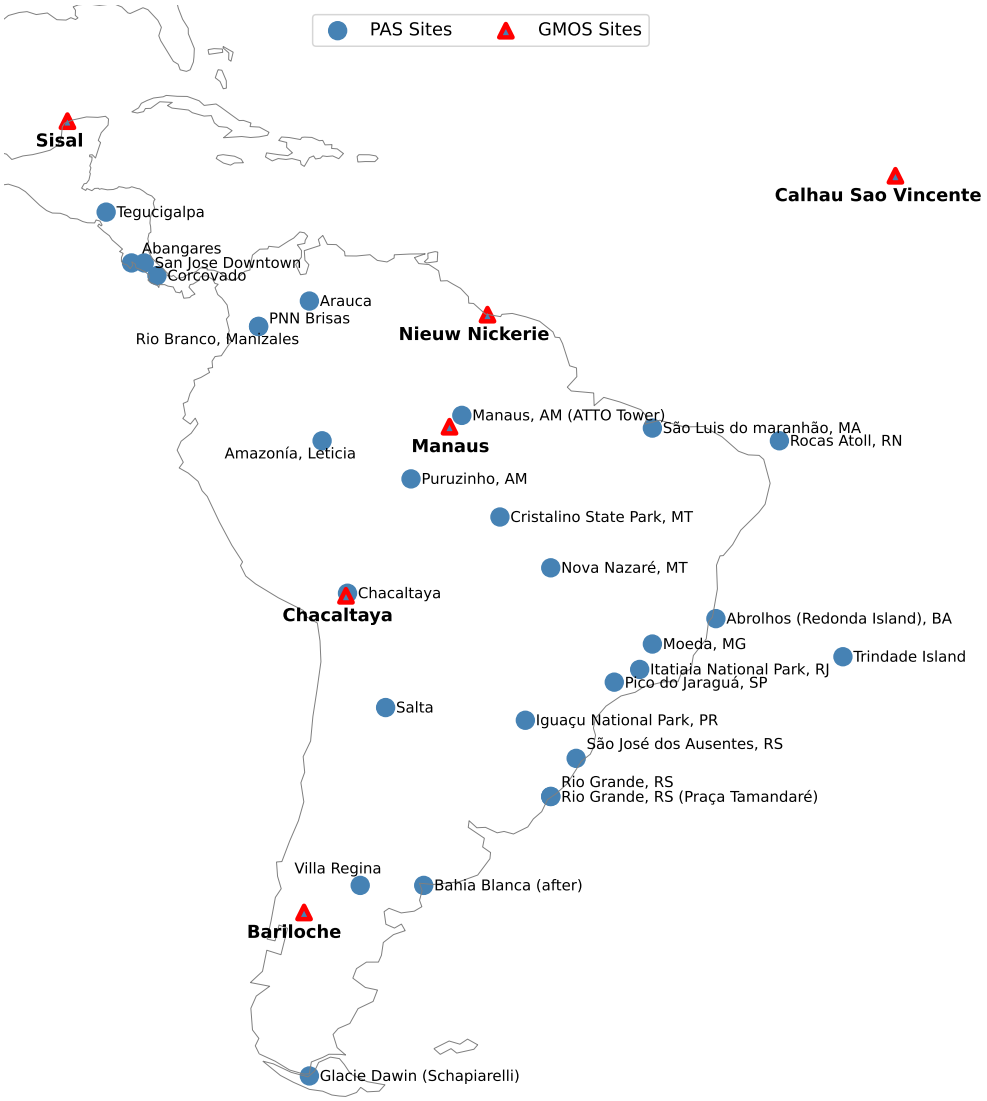

Figure 2-2: Map showing the names and locations of the GMOS Monitoring Network Sites and Passive Sampler sites in Latin America. GMOS sites are indicated by the red triangles, and the PAS sites are indicated by the blue dots[27, 34].

2.2.4 Pre-processing and Comparison of Observed and Modeled Mercury Concentration in the Atmosphere

Annual average GEM concentration data for 27 PAS sites in Latin America was obtained from Quant et al.[27], which included information about the coordinates of the deployment sites and the period of measurement. The PAS data was already ngm^{-3} hence there was no need for pre-processing before comparison with the modeled Hg concentrations. Furthermore, the PAS had been deployed for a year; the different deployment dates ranged from October 20th, 2017, to March 14th, 2020. Therefore the annual average GEM concentrations from the PASs were

compared to the modeled annual average Hg^0 for 2015 for each site.

Available Hg observation data from the GMOS stations on Figure 2-2 was obtained from the GMOS online database (http://www.gmos.eu), as well as published studies about the Hg monitoring data from the different sites [19, 34]. The data sets were pre-processed based on the information in Sprovieri et al.[19] and Koenig et al.[34]. Daily and annual averages of the observed TGM concentration were calculated to compare with the GEOS-Chem output.

2.3 Results and Discussion

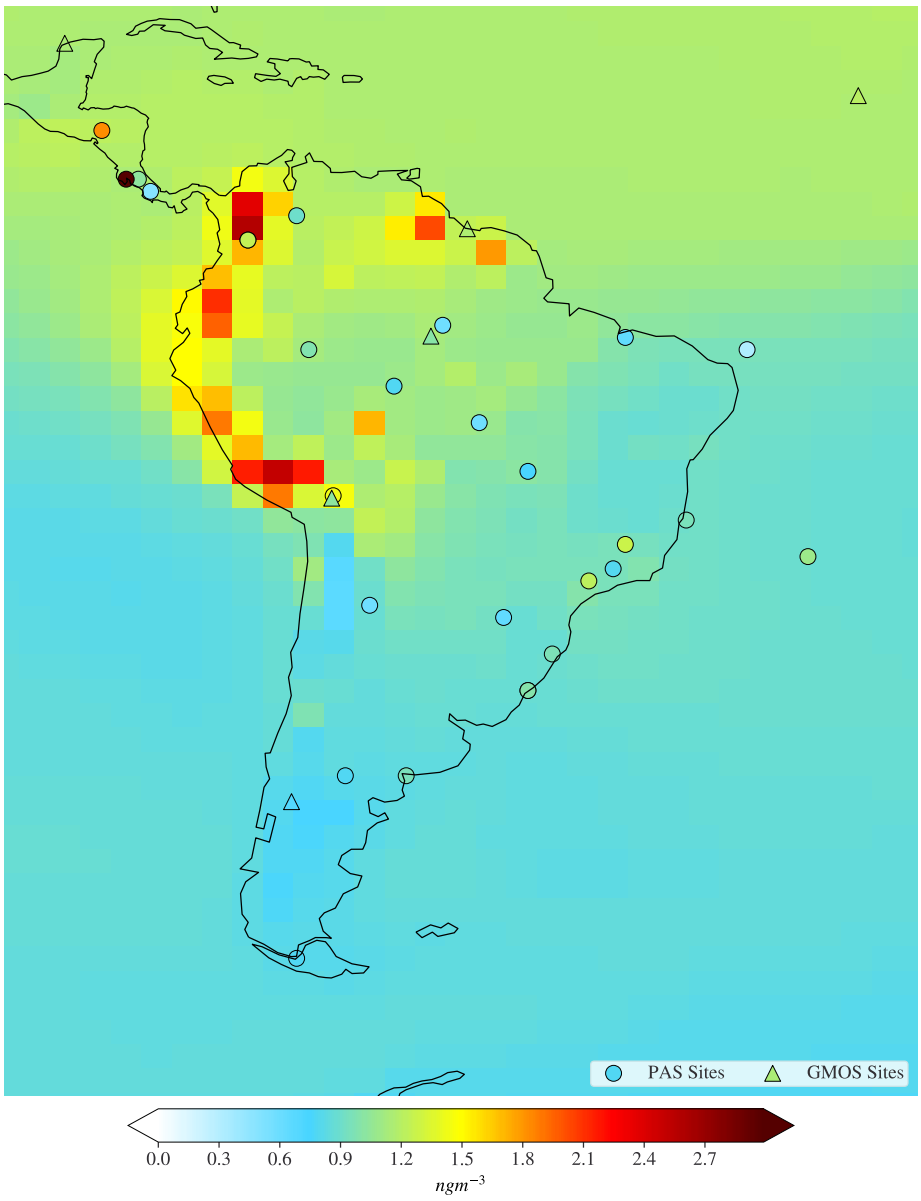

Figure 2-3: The average annual Hg concentration on Latin America's surface. The background is the yearly average Hg^0 concentration generated by the Base (ASGM=ON) simulation for 2015. Circles represent the annual average GEM concentration at PAS sites, while triangles represent the yearly average TGM concentration at GMOS sites[19, 27, 34].

Recent publications analyzing global Hg monitoring data highlight an observed inter-hemispheric gradient of Hg concentration where Hg concentration in the southern hemisphere is lower than Hg concentration in the northern hemisphere[3, 19]. The gradient is evident in the simulated background annual average Hg^0 concentration as seen in Figure 2-3. Moreover, most GMOS sites agree with and validate the modeled interhemispheric gradient.

However, a glance at Table 2.3 shows that the model overestimates the annual average Hg concentration at all the GMOS sites. Moreover, Figure 2-4 better visualizes the difference between the modeled and observed concentrations. The bar chart in Figure 2-4 compares observed and modeled Hg concentrations at the GMOS sites. Observed concentrations are indicated in red, modeled in blue, and ASGM contribution in green. There are annotations on the bars indicating the average concentration of Hg. In addition, each bar is annotated above with the data set's standard deviation and error bars.

Table 2.3: Comparison of the modeled Hg^0 concentration and the observed TGM concentrations at the GMOS sites. The percentage difference between the model predictions and the observations depicts the extent to which the model predicts the observed TGM concentrations

GMOS Site	Observed Average TGM/GEM Concentration (ngm^{-3})	Modeled Average Hg^0 Concentration (ngm^{-3})	Percentage difference between modeled and observed average (%)	Percentage ASGM Contribution (%)
Sisal	1.15	1.26	10	9
Calhau	1.22	1.29	6	9
Nieuw Nickerie	1.17	1.41	20	16
Manaus	1.01	1.26	25	18
Chalcataya	1.04	1.21	17	23
Bariloche	0.71	0.9	27	6

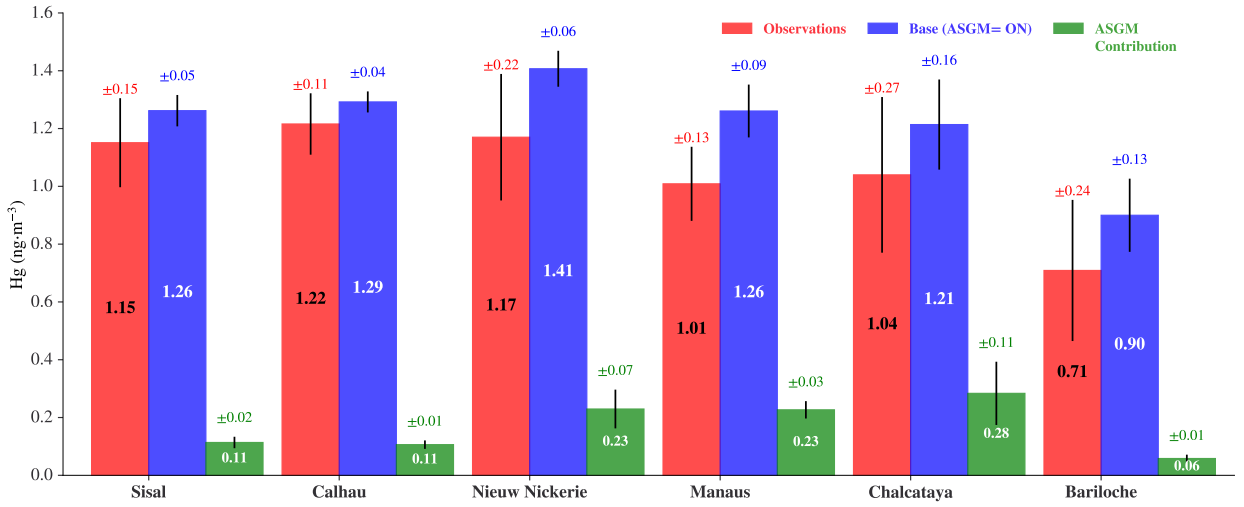

Figure 2-4: Bar chart comparing the modeled and observed average Hg concentration at the respective GMOS Sites. The blue bars indicate the modeled annual average concentration, the red bars indicate the observed annual average concentration, and the green bars indicate the ASGM contribution at each site. The bars are annotated with the average Hg concentration values. Moreover, the error bars and the annotated value above the bars show the standard deviation in each data set.

Figure 2-4 shows that ASGMs modeled contribution is low in most sites except for Chacaltaya, Manaus, and Nieuw Nickerie. The model's behavior regarding the predicted ASGM contribution at these sites is not surprising since these three sites are in countries estimated to be among the top 10 Latin American ASGM Hg emitters in the ASGM emission inventory used for GEOS-Chem simulation. Even though the model estimates a notable ASGM contribution at the Manaus (18%) and Nieuw Nickerie (16%) sites, the sites lack enough data to fully characterize the ASGM contribution to the modeled Hg^0 concentration over the long term. However, the predicted ASGM Hg contribution at Chacaltaya is the highest at 23% as seen in Table 2.3.

As far as the PAS observed GEM concentrations are concerned, the modeled background Hg^0 concentrations in Figure 2-3 seem to match the PAS GEM measurement at Chalcataya, but, according to Quant et al.[27], the higher GEM levels observed at Chacaltaya (1.4 ngm^{-3}) are likely to reflect a known Hg spill near the sampling site and may not reflect regional Hg concentration values. The Chacaltaya Hg spill occurred after the GMOS Chacaltaya site had completed its data collection period. Thus, the GMOS Chacaltaya station's annual average Hg concentration reflects regional Hg concentration more than the PAS station. In comparison with PAS data, the GEOS-Chem model also overestimated atmospheric concentrations. This phenomenon is more prevalent in inland sites than coastal ones.

In the Amazon region, for example, there is a difference between the model and inland PAS sites. This may be because the GEOS-Chem model version used in this study underestimates Hg uptake by plants [35], which means that the model predicts a higher Hg concentration in the atmosphere than it is. Figure 2-5 which shows the modeled (blue circles) and observed (red circles) annual average Hg^0 plotted as a function of latitude indicates the interhemispheric gradient observed in GEOS-Chem. The observation error bars represent the replicate precision of the observations, while the model error bars represent the 95^{th} percentile range bootstrap confidence interval for the mean annual Hg^0 .

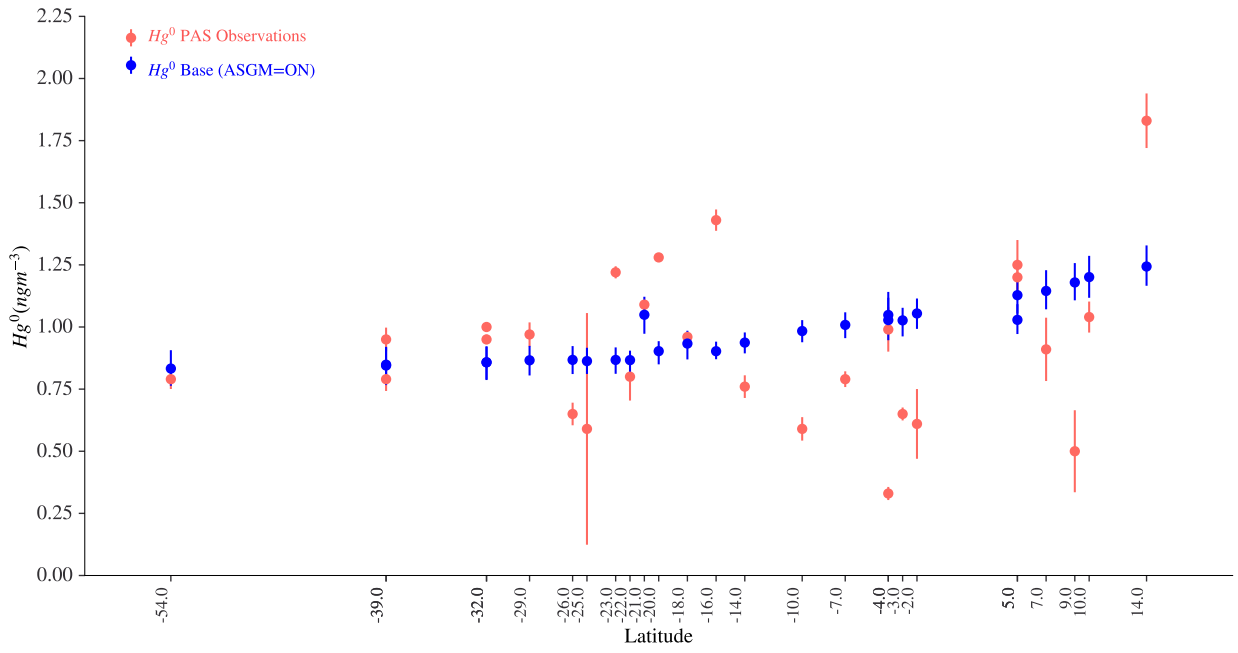

Figure 2-5: Hg Concentration in the atmosphere as a function of Latitude. The Base (ASGM = ON) simulation (blue circles) and observed (red circles) annual average Hg^0 plotted are plotted as a function of latitude to evaluate spatial trends across the continent. The observation error bars represent the replicate precision of the observations while the model error bars represent the 95^{th} bootstrap confidence interval for the mean annual Hg^0 .

GEOS-Chem's overestimation of Hg concentration in the Amazon region observed above was also addressed in Feinberg et al.[35] where GEOS-Chem simulations were compared with litterfall, throughfall, and flux tower measurements from 93 forested sites to evaluate vegetation as a Hg sink. The study concluded that the GEOS-Chem version, 12.8.1 underestimates Hg^0 dry deposition, which may explain why measurements of Hg concentration in Latin America were lower than predicted by GEOS-Chem .

2.3.1 Modeled vs. Observed Temporal Trends

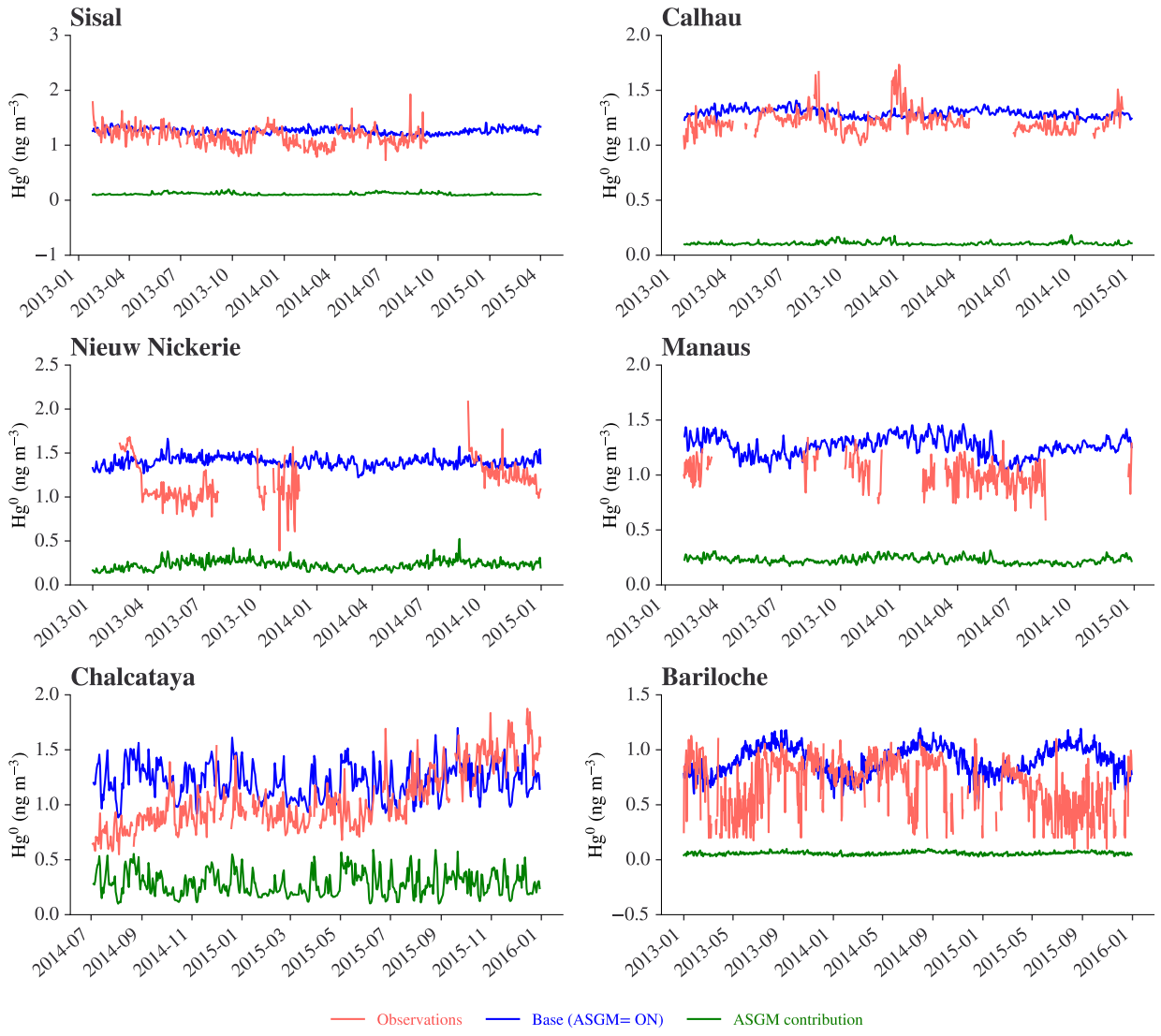

Figure 2-6: Time series plots of the observed TGM concentrations at different GMOS sites in red with the corresponding modeled concentration in blue and the associated ASGM contribution in green. Except for the CHC site, where the data are from July 2014 and January 2016, the available data and corresponding model outputs were plotted between January 2013 and January 2016.

This study also compared observed and modeled data on a daily resolution as seen in Figure 2-6, which shows the time series of the modeled Hg^0 concentration in the atmosphere alongside the observed Hg and the simulated ASGM contribution to the atmospheric Hg concentration at the GMOS sites. The GEOS-Chem model version used in this study overestimated the concentration of Hg on most days. However, the GEOS-Chem estimated average Hg^0 concentration over the available observation period was within one standard deviation of the observed Hg in most of the sites except for the Manaus and Nieuw Nickerie sites. GEOS-Chem's overestimates the

observed GEM concentrations at the Manaus and Bariloche master sites by over 25% and the GEM concentration at Nieuw Nickerie by 20%, which may be indicative of poor parameterization of GEM in the model. Moreover, the overestimation of GEM concentrations in Manaus further indicates the model's poor implementation of Hg plant uptake through dry deposition, as discussed in Feinberg et al.[35].

Figure 2-7 displays the scatter plots of modeled Hg concentrations as a function of the observed Hg concentrations for each site. Each plot uses the red line to evaluate the linear relationship between the modeled and observed Hg concentrations. Equations of the red regression line and the coefficient of determination for each site are also displayed on the plots. The general observation is that the model poorly matched the observations, indicated by the mild and even flat slopes and shallow R^2 values. The low correlations between the model and observations may be attributed to poor vegetation uptake[35]. Another plausible hypothesis about the poor model prediction is that the input ASGM emissions that GEOS-Chem uses are poorly parameterized. Wrong emissions in the model may reduce the extent to which the model recreates the observed atmospheric Hg concentrations. Chapter 3 investigates this hypothesis in detail and highlights some causes, such as the underestimation of emissions from high Hg-emitting regions like Madre de Dios.

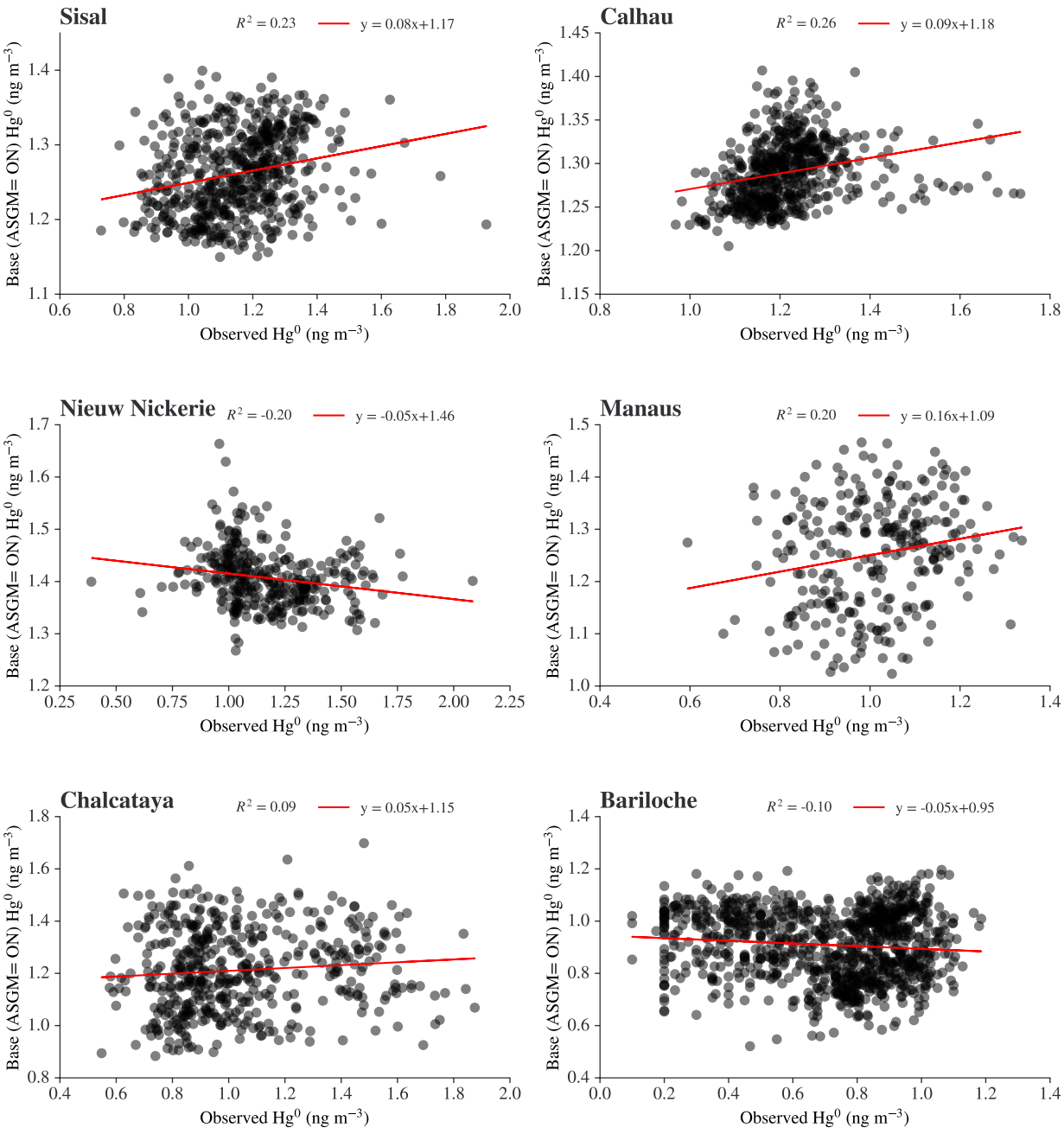

Figure 2-7: Scatter plots of the modeled Hg concentration as a function of the observed concentration. The red line is used to investigate the extent of the linear relationship between the modeled and observed Hg concentrations. The coefficient of determination(R^2) and the equation of the red regression line are shown above each site scatter plot

2.3.2 Comparison of Model Predictions

GEOS-Chem's skill in reproducing the Hg concentration measured using the two sampling methods was analyzed using the scatter plots in Figure 2-9. Figure 2-9 (a) shows the modeled annual mean Hg^0 concentration for each GMOS site as a function of the observed Hg^0

concentration at the site, while Figure 2-9 (b) shows the modeled annual mean Hg^0 concentration for each of 6 PAS sites that are the closest to the 6 GMOS sites in (a) as a function of the observed Hg^0 concentration at the respective site. In each plot, the red line is the regression line to investigate the strength of the association between the modeled concentrations and observed concentrations.

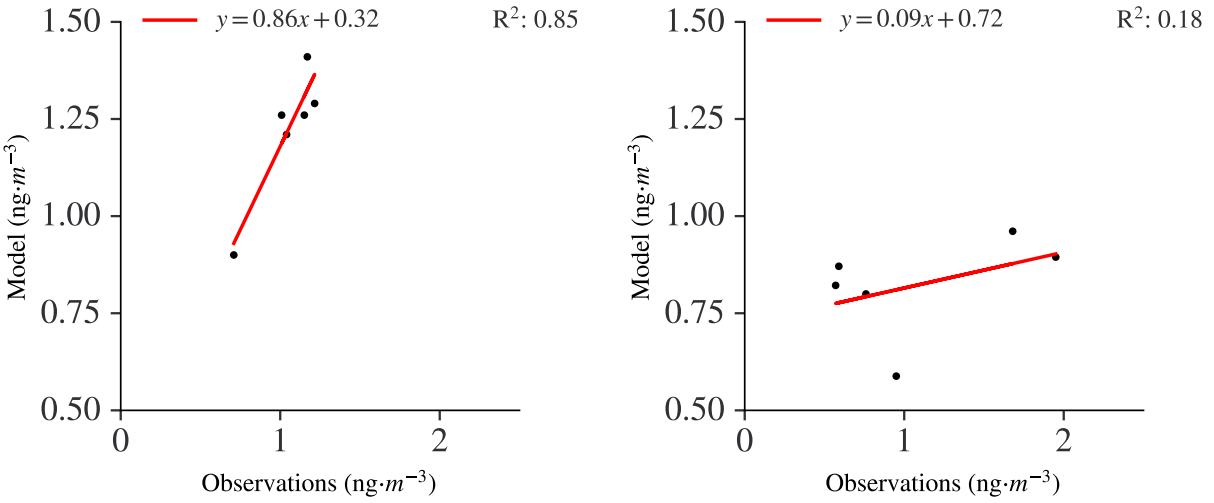

(a) GMOS (b) PAS

Figure 2-9: Scatter plots comparing model's predicted Hg Concentration means with the GMOS and PAS average annual Hg Concentration means. (a) shows modeled annual mean Hg^0 concentration for each site as a function of the observed Hg^0 concentration at the site. The red line is the regression line

Figure 2-9 shows that GEOS-Chem is better at reproducing the actively monitored average Hg concentration (steep slope and large R^2) than the data from the passive monitoring. Furthermore, adding all the remaining Hg concentrations from the PAS did not improve the slope or R^2 but worsened the relationship. Even though Figure 2-7 informs us that GEOS-Chem poorly predicted daily averages at the individual GMOS sites, Figure 2-9 shows that its predictions of actively monitored Hg concentrations are better in aggregate than passively monitored Hg concentrations. This result suggests that modeling studies would gain better insights from comparisons with actively monitored Hg concentrations. However, this result does not render PAS monitoring obsolete. Using PAS technologies, we can obtain high-quality data about Hg concentrations in the atmosphere and understand regional background Hg concentrations over long periods. Since PAS networks are relatively inexpensive and easy to install, countries can use them to understand their Hg emissions better, providing valuable

global and regional monitoring data. A better understanding of temporal trends can be gained from active monitoring, as evidenced by the analysis of GMOS TGM concentrations. Furthermore, a single data set of actively monitored Hg concentrations can be analyzed to generate metrics such as mean, iqr , and 95^{th} percentile range , allowing multiple ways to compare modeled and observed concentrations. Despite not recreating the exact Hg concentrations observed at GMOS sites, improvements to the model, such as the update in the model's dry deposition discussed in Feinberg et al.[35] may improve the GEOS-Chem's predictions of measured Hg concentration in the atmosphere. Additionally, Shah et al.'s[23] improved mechanistic model of the atmospheric redox chemistry of mercury may also reduce GEOS-Chems's error in predicting the observed concentrations.

2.4 Conclusion

This chapter explored the relationship between the modeled and observed Hg concentrations in Latin America. The atmospheric Hg measurements from six active monitoring sites across Latin America part of the GMOS network were analyzed and compared with modeled Hg^0 concentrations at the respective sites[34, 19]. Furthermore, annual average GEM measurements from 27 PAS sites across Latin America were compared to 1-year beverages for Hg^0 concentrations at the respective monitoring sites [27]. A relatively weak relationship was found between the observed mercury species (GEM and TGM) and those in the Base (ASGM = ON) simulation , demonstrating a need for improving the models. Additionally, GEOS-Chem recreated the average Hg concentration measurements from active monitoring stations better than PAS. Lastly, improved vegetation uptake and more accurate emission parameterizations may improve the model's prediction.

Chapter 3

Top-down Constraints on Atmospheric Mercury Emissions from ASGM Activities

To measure the effectiveness of mitigation and elimination strategies for reducing Hg pollution from ASGM, Hg emissions estimates will be compared to baseline estimates per Article 22 of the MC. The ASGM industry is often unregulated, with little government oversight and a limited amount of reliable data[36]. Therefore, measurement of Hg use in the ASGM sector is difficult due to its complexity and largely informal nature. Typically, finding reasonable estimates of ASGM Hg use, gold production, and staff requires extensive site visits, multiple interviews, observations, and measurements at ASGM sites[36].

In this chapter, we apply a top-down approach at a regional scale to estimate ASGM Hg emissions (emission inversion) from Peru. As of now, there has been no scientific study using Hg atmospheric monitoring data and atmospheric models to provide top-down constraints for ASGM emissions. Section 3.2 describes the overall methodology. We combine ground-based observations of atmospheric Hg from the case study region[34], a national inventory for Peru[37] and simulations with the GEOS-Chem global CTM. Reference (also known as a priori) emissions are from the GMA 2018[3, 33]. The Markov Chain Monte Carlo is the inversion method used (Sect. 3.2.5) to obtain the optimized (a posteriori) emissions, considering uncertainties associated with reference and ground-based observations. Section 3.3 presents results and discussion. Comparisons of observations and model outputs are given in Sect. 3.3.3. The optimized emissions from 5 regions in Peru are shown in Sect.3.3.4. Finally, we discuss the implications of the inversion results for providing baseline estimates of ASGM Hg emissions

and summarize conclusions (Sect. 3.4).

3.1 Background

Numerous prior studies have quantified anthropogenic Hg sources, including ASGM Hg emissions using different methodologies. Bottom-up estimates leverage collected data on underlying activities and emission factors to estimate regional and global totals. For instance, the bottom-up global inventory in the GMA 2018 estimated ASGM Hg emissions to be 838 Mg with an uncertainty range of 675-1000 Mg for 2015 [3, 33]. Moreover, Streets et al. (2019) tested six different proxies for scaling emissions to other years and used an average value to scale the inventory of emissions to the year 2015, thus estimating that ASGM was the largest source and responsible for 775 Mg of emissions[38]. Muntean et al. (2014) also used a bottom-up technique in which they found that poverty in gold ore-rich countries (as measured by the GINI index [39], where available) was correlated with data on ASGM production activity. The poverty-based approach they used estimated that ASGM was responsible for 728.27 Mg emissions in 2010, equivalent to 41.1% of the global Hg emissions[40]. Such inventories are essential and a critical input to model Hg using CTMs such as GEOS-Chem .

However, the different assumptions on the activity data and emission factors induce significant uncertainty in the emission inventories. Furthermore, the bottom-up approach has biases due to its reliance on officially reported emission data, which may cause regional and national differences in accuracy. Countries identify and quantify Hg sources released within their borders through national baseline Hg-use estimates as per O'neill and Telmer[36]. Under Article 7 of the MC and Annex C, countries must include in their NAPs baseline estimates of the quantities of mercury used in ASGM within their territory[41].

In contrast to bottom-up approaches, top-down emission estimation approaches combine atmospheric transport and chemistry models with atmospheric concentration measurements to quantify emissions. Even though the atmospheric chemistry literature has various top-down method applications, no study explicitly constrains ASGM Hg emissions. For instance, Bousquet et al., 1999 applied top-down methods to infer surface fluxes of atmospheric CO_2 from observed concentrations[42]. Furthermore, Kopacz et al., 2009, employed top-down techniques to quantify source contributions to ozone pollution at two adjacent sites on the U.S. west coast in

the spring of 2006[43]. They used GEOS-Chem as a common intercomparison platform to show global consistency between the satellite data sets and the in situ data. This underscores the role models such as GEOS-chem have as integration platforms for differently sourced data to generate unified insights. Likewise, Hg emissions have been constrained using top-down methods in Song et al., 2015 where a top-down approach at a global scale is applied to quantitatively estimate present-day Hg emission sources and critical parameters in GEOS-Chem to better constrain the global biogeochemical cycle of Hg[44]. Moreover, Denzler et al., 2017 used a top-down approach to quantify Hg emissions on a European scale based on the atmospheric Hg measurements conducted at the remote high-altitude monitoring station, Jungfraujoch, Switzerland[45].

3.2 Methods

Chapter 2 of this thesis discussed the differences between the GEOS-Chem model predictions of Hg at various monitoring stations and in Latin America. In one hypothesis, the difference between the model and the observations was attributed to how the emissions were parameterized in GEOS-Chem . Generally, the input emissions in GEOS-Chem are determined by the Hg inventory used; hence, we first evaluated the Hg inventory used in the simulations in Chapter 2 (GMA 2018, also called AMAP/UNEP 2015 inventory) against other global inventories. Next, the inventory was compared to a national inventory for Peru developed by the Artisanal Gold Council in preparation for Peru's NAP [17]. Once the differences between the GMA 2018 inventory[33] and the Peruvian national inventory were analyzed [17], the global inventory was re-gridded to the GEOS-Chem grid, and the emissions from grid boxes corresponding to different departments in Peru were scaled. The scaled inventories were used to create the simulations described in Table 3.1. These simulations were used to investigate the sensitivity of the Hg concentration at distant locations to the changes in emissions from the grid boxes in the case study region. The simulated Hg^0 concentration in the atmosphere was compared to the observed TGM concentration in the atmosphere to determine the sensitivity of the Hg^0 concentration to the changes in emissions from individual grid boxes and multiple grid boxes.

3.2.1 Mercury Emission Inventories

Globally gridded emissions inventories such as those shown in Figure 3-1 are a critical input to CTMs such as GEOS-Chem . Figure 3-1 shows the distribution of Peruvian anthropogenic Hg emission estimates by different global inventories [3, 33, 38, 40]. The GMA 2018 ASGM Hg emissions estimates for 2015 are shown in Figure 3-1, (a). The ASGM Hg emissions in the GMA 2018 inventory were distributed by assigning emission estimates to geo-located point sources, using reported emissions information where available, and otherwise assigning a modeled emission to the point. Emissions that could not be assigned to point sources were distributed using sector-specific proxies [33]. The proxies for ASGM Hg emissions in Peru were the locations of legal mining concessions and the global alluvial gold map data set. This inventory estimated that ASGM was responsible for about 110 tonnes of annual emissions in Peru. Moreover, the GMA 2018 inventory was used in all the GEOS-Chem simulations conducted in this study. This inventory was used because it was more representative of the ASGM emissions than the other two inventories, as the total Hg emissions are compatible with bottom-up baseline ASGM Hg emissions. Figure 3-1,(b) shows how anthropogenic Hg emissions were distributed in the EDGAR ASGM Hg emissions inventory[40]. This global mercury emissions inventory includes emissions from all key mercury emitting sources, and Peru's total Hg emissions estimate was about 26 tonnes per year. Finally, Figure 3-1,(c) shows how anthropogenic Hg emissions were distributed in the Streets et al. 2019 Hg emissions inventory[38]. They analyzed the global and regional trends in anthropogenic Hg releases to the atmosphere between 2010 and 2015 and the associated trends in modeled and measured Hg concentrations at sites around the world. Their Peru total Hg emissions estimate was about 40 tonnes per year.

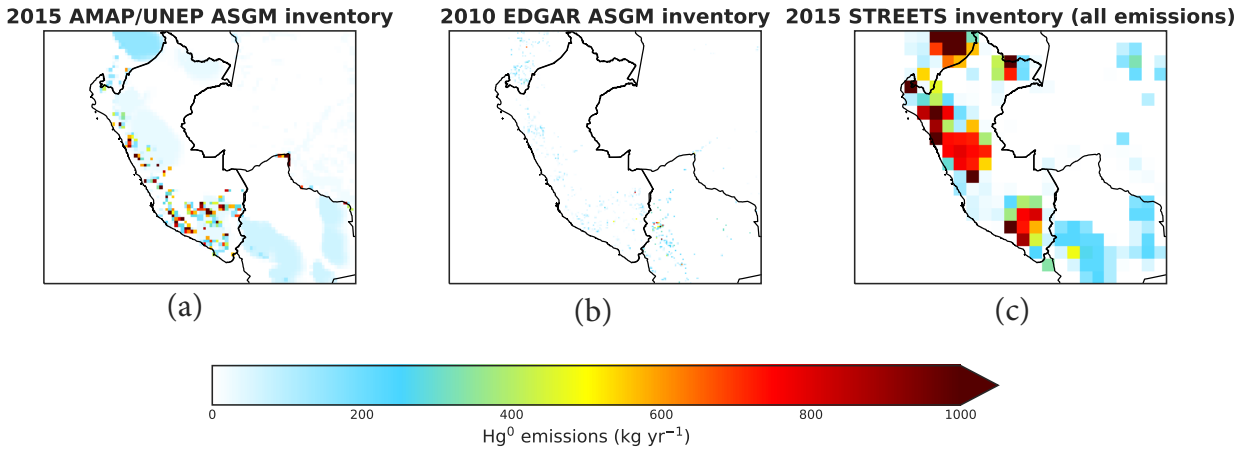

Figure 3-1: Comparison of Hg emissions from Peru as estimated by different global inventories [3, 33, 38, 40].

3.2.2 Emission Modification and GEOS-Chem Simulations

Five more simulations were added to the Base (ASGM = ON) simulation and No ASGM (ASGM = OFF) simulation GEOS-Chem simulations presented in Chapter 2. The other five simulations were sensitivity runs that used modified emission inventories corresponding to changes in emissions from one of the grid boxes in the case study region.

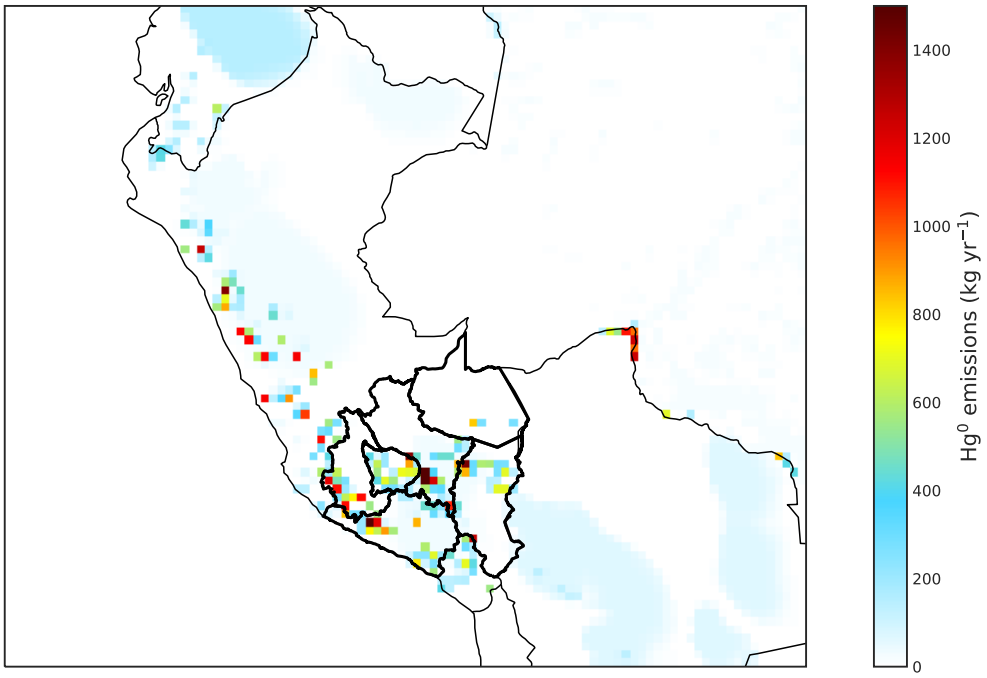

(a) GMA 2018 (AMAP/UNEP 2015) inventory Grid Resolution

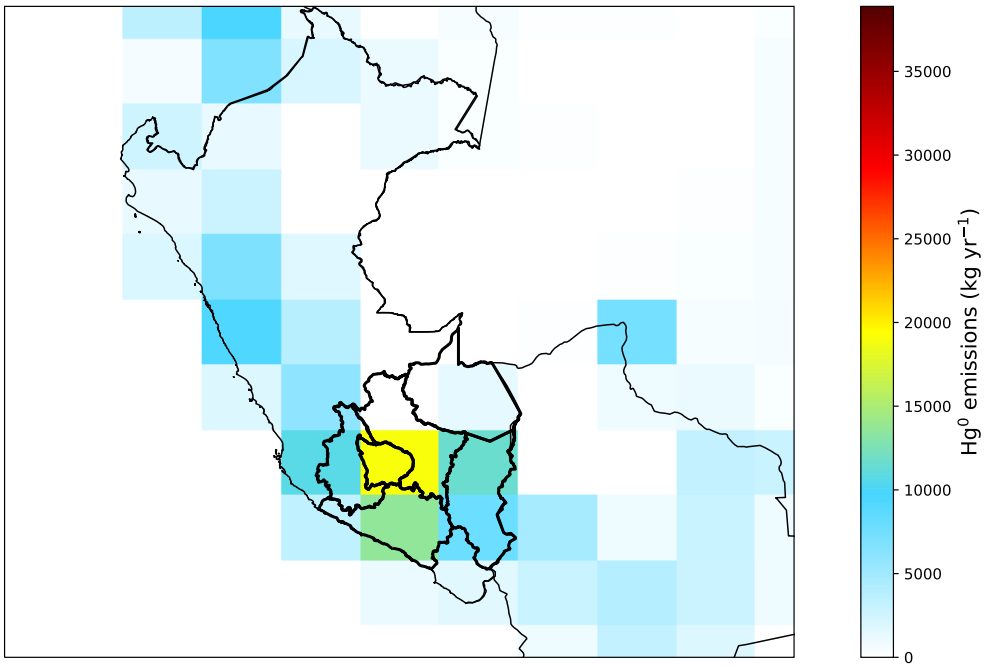

(b) GEOS Chem Model Grid Resolution

Figure 3-3: Maps showing how the GMA2018 emission estimates for the year 2015 were distributed for Peru before re-griding (a)[33] and after re-gridding to the GEOS-Chem grid (b)

Table 3.1: Table showing the different GEOS-Chem simulations used in the analysis

Simulation Name	Resolution	**Description Estimate**
Base (ASGM=ON)	2.0×2.5	All Hg anthropogenic emission sources are turned on
No ASGM (ASGM=OFF)	2.0×2.5	All ASGM emissions are turned off
Mdd	2.0×2.5	Emissions from the GEOS-Chem grid box located in Madre de Dios were scaled up by a factor of 2
Apr	2.0×2.5	Emissions from the GEOS-Chem grid box located in Apurimac were scaled down by a factor of 0.5
Aqp	2.0×2.5	Emissions from the GEOS-Chem grid box located in Arequipa department were scaled up by a factor of 2
Npun	2.0×2.5	Emissions from the GEOS-Chem grid box located in the northern region of Puno were scaled up by a factor of 2
Spun	2.0×2.5	Emissions from the GEOS-Chem grid box located in the southern region of the Puno were scaled up by a factor of 2

3.2.3 Simulated Atmospheric Mercury Concentration Signals

The relationship between the Hg^0 emissions from a specific grid box and the GEOS-Chem simulated atmospheric Hg^0 concentration at distant points from the emissions source is assumed to be defined by a linear function. This means that an increase in emissions is expected to increase the Hg^0 concentration. Consequently, the relationship between emissions and concentrations can be represented by the following equation:

$$Hg^0_{sig(region)} = Hg_{m_0} + \frac{(Hg_{m_1} - Hg_{m_0})}{(m_1 - m_0)}(m_{(region)} - m_0) \tag{3.1}$$

where:

$region$ is the location of the emission source within the case study region.

$Hg^0_{sig(region)}$ is the simulated Hg^0 concentration at the observation site due to $m_{(region)}$ at the grid box in the specific $region$ of interest.

Hg_{m_0} is the Hg concentration at the observation site generated by the Base (ASGM =ON) simulation.

Hg_{m_1} is the Hg concentration at the observation site generated by the i^{th} region simulation i=Mdd,Apr, Aqp,Npun,Spun.

m_1 is the amount of emissions in tons after scaling the emissions from a specific grid box.

m_0 is the amount of emissions in tons before scaling the emissions from a specific grid box.

3.2.4 Observation Site Selection

TGM and GEM observation data from different locations in Latin America were analyzed and compared to the GEOS-Chem simulated Hg^0 concentrations for those sites in Chapter 2. The GEOS-Chem predictions for ASGM contributions to atmospheric Hg concentration were higher at the CHC, making it an excellent candidate to use as a reference for comparison with the modified GEOS-Chem Hg concentration predictions. Moreover, this site is the closest monitoring site to Peru hence it is expected that it would be more likely to detect atmospheric

Hg^0 changes that result from the changes in Hg emissions from the case study region. The time series of the observed concentration at the CHC station between July 2014 and January 2016 is shown in Figure 3-4. The red line indicates the daily average concentration, while the grey line shows the 120-day moving average, which highlights the upward trend in the daily averages.

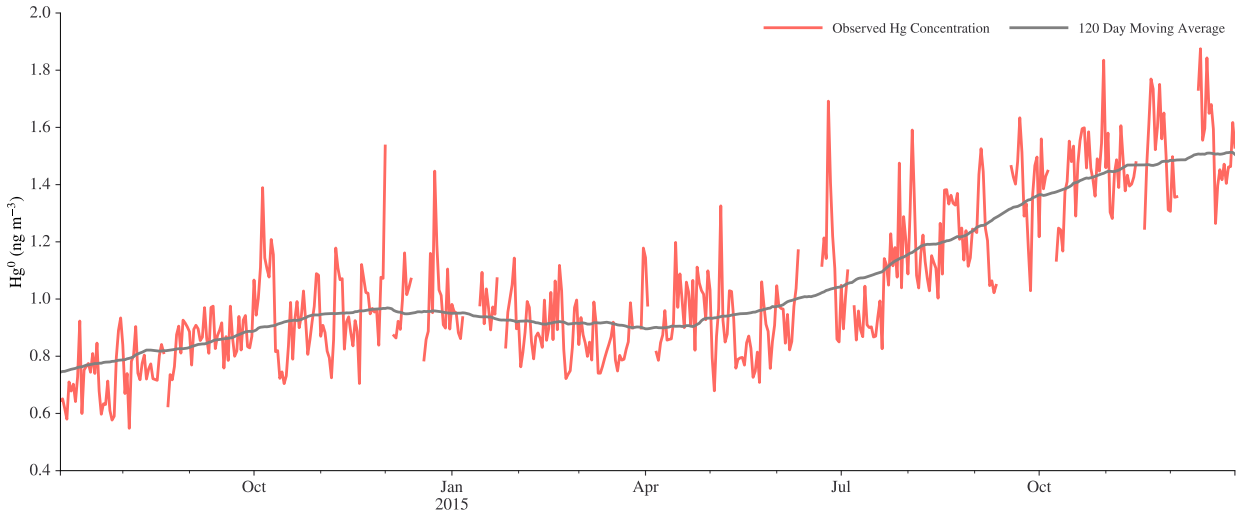

Figure 3-4: The average daily TGM concentration at CHC in ng m^{-3} as a function of time over the measurement period from July 2014 to January 2016[34]. The red line indicates the daily average concentration, while the grey line shows the 120-day moving average, which highlights the upward trend in the daily averages.

The detailed characteristics of the observations over this measurement period were described in Koenig et al.[34]; hence my analysis focused on using the observation TGM data to evaluate the performance of the GEOS-Chem model in predicting the Hg^0 based on the input Hg^0 emission inventories. As shown in Figure 3-4, the TGM concentration at CHC showed an upward trend, which Koenig et al. (2021) attribute to El Niño-Southern Oscillation (ENSO)[34]. As a result, they categorized the measured TGM concentrations in the atmosphere at the CHC site as normal conditions (NC), 2014-07 to 2015-05, and ENSO conditions from 2015-06 to 2016-01. To reduce the number of records associated with ENSO, we limited our analysis to one year's worth of data from 2014-07 to 2015-07.

3.2.5 Inverse Modelling with Markov Chain Monte Carlo

Inverse modeling is described by Brasseur, and Jacob [29] as a method for quantifying variables that drive a physical system using observations. Accordingly, the variables are statistically

optimized based on the observational and other information available. Variables we wish to optimize are called state variables and assembled into a state vector x. In the same way, the observations are assembled into an observation vector y. The forward model F of the physical system describes the relationship between x and y:

$$y = F(x, p) + \epsilon_0 \tag{3.2}$$

where:

p contains all variables in the model that we will not optimize as part of the inversion

ϵ_0 a vector of observations errors, which includes errors from measurements, the forward model, and model parameters

Forward models describe the effects of the system as functions of the cause x, usually by using equations that describe the system's physics. The cause (x) can be quantified via inversion of the model based on the effect (y). Moreover, x is estimated with some statistical error when $\epsilon_0 \neq 0$ is present. The solution for x is called the optimal estimate, posterior estimate [29].

The uncertainty in obtaining x from y requires us to consider constraints on the value of x called priors that could reduce the error on the optimal estimate. We generally use the prior estimate x_A as a constraint, representing our best estimate of x before the observations. The GMA 2018 inventory estimates of the emissions from the respective grid boxes are used as priors for our analysis. The prior estimate x_A has some error ϵ_A. As a result, the ideal estimate must consider the relative information given by the observations y and the prior estimate x_A. In inverse modeling, we can analyze the relative importance of observations and prior knowledge. In this way, it provides insight into the effectiveness of an observing system in constraining x (Hg emissions) [29].

For this analysis, we use the measured Hg concentration (observation vector y) to constrain the emissions from grid boxes in the case study region (state vector x). The forward model is given by the linear combination of the signals generated by the GEOS-Chem model as shown in Equation 3.3 below:

$$Hg_{conc} = Hg_{m(MdD)} + Hg_{m(S-Puno)} + Hg_{m(N-Puno)} + Hg_{m(Apr)} + Hg_{m(Aqp)} + Hg_{m_0} + \epsilon \tag{3.3}$$

where:

$Hg_{m(MdD)}$ is the Hg concentration signal resulting from emissions from the Madre de Dios (MdD) grid box.

$Hg_{m(S-Puno)}$ is the Hg concentration signal resulting from emissions from the South Puno (S-Puno) grid box.

$Hg_{m(N-Puno)}$ is the Hg concentration signal resulting from emissions from the North Puno (N-Puno) grid box.

$Hg_{m(Apr)}$ is the Hg concentration signal resulting from emissions from the Apurimac (Apr) grid box.

$Hg_{m(Aqp)}$ is the Hg concentration signal resulting from emissions from the Arequipa (Aqp) grid box.

Hg_{m_0} is the baseline Hg concentration signal.

ϵ is the error in the prior estimates.

Each of the $Hg_{m(region)}$ terms of Equation 3.3 represent signals from the different departments are calculated using Equation 3.1 an the form the parameter vector p. The $m_{(region)}$ terms are the only unknowns and the equation can be expanded to isolate the terms with $m_{(region)}$, which is the parameter we are optimizing for in the inverse modeling method. The expanded form of Equation 3.3 is shown below:

$$\begin{aligned} Hg_{conc} = {} & (m_{(MdD)}Hg_{sig_{(MdD)}} - m_o Hg_{sig_{(MdD)}}) + (m_{(S-Puno)}Hg_{sig_{(S-Puno)}} - m_o Hg_{sig_{(S-Puno)}}) \\ & + (m_{(N-Puno)}Hg_{sig_{(N-Puno)}} - m_0 Hg_{sig_{(N-Puno)}}) + (m_{(Apr)}Hg_{sig_{(Apr)}} - m_o Hg_{sig_{(Apr)}}) \\ & + (m_{(Aqp)}Hg_{sig_{(Aqp)}} - m_o Hg_{sig_{(Aqp)}}) + Hg_{m_0} + \epsilon \end{aligned} \tag{3.4}$$

Since the values of $m_{(region)}$ are the state variable we want to estimate, they can be represented as $\theta_i = m_{(region)}, i = 1$ and the other terms, including the background concentration and error, are combined into one constant, C:

$$\begin{aligned} Hg_{conc} = \theta_0 C + \theta_1 Hg_{sig_{(MdD)}} + \theta_2 Hg_{sig_{(S-Puno)}} + \theta_3 Hg_{sig_{(N-Puno)}} \\ + \theta_4 Hg_{sig_{(Apr)}} + \theta_5 Hg_{sig_{(Aqp)}} \end{aligned} \tag{3.5}$$

$$Hg_{conc} = \begin{bmatrix} C & Hg_{sig_{(MdD)}} & Hg_{sig_{(S-Puno)}} & Hg_{sig_{(N-Puno)}} & Hg_{sig_{(Apr)}} & Hg_{sig_{(Aqp)}} \end{bmatrix} \times \begin{bmatrix} \theta_0 \\ \theta_1 \\ \theta_2 \\ \theta_3 \\ \theta_4 \\ \theta_5 \end{bmatrix} \tag{3.6}$$

where $\theta_0 = 1$ and Hg_{conc} is the modeled Hg concentration at the observation site of interest.

The Markov-Chain Monte Carlo (MCMC) is a valuable sampling method for fitting models to data[46]. We apply the MCMC to constrain ASGM Hg emissions from the case study region in Peru. The model is generated by a set of parameters and emissions, and we aim to sample from the parameters that best fit our data. The MCMC compares the modeled concentrations to the observed data using metrics such as the 95^{th} percentile range confidence interval, mean, and the iqr . The MCMC models the given data by sampling around optimum values from the posterior distribution. The MCMC is a Bayesian approach; hence it requires the definition of priors on the parameters of interest. The priors encode information that we already know of the system. The probability of the model given the observed data is given by the posterior probability, $P(\theta|D)$, which is calculated using the Bayes theorem:

$$P(\theta|D) = \frac{P(D|\theta)P(\theta)}{P(D)} \tag{3.7}$$

where:

$P(D|\theta)$ is the likelihood which is the probability of the data given the model

$P(\theta)$ is the prior, which is the probability of the model and

$P(D)$ is the evidence which is the probability of the data.

Bayes' theorem relates posterior the probability distributions of parameters ($f_{post}(\theta, D)$) to the likelihood function ($f(D|\theta)$) and prior knowledge of the parameter distributions ($f_{prior}(\theta)$)

The MCMC with the Metropolis-Hastings algorithm enables the estimation of the sampling of the posterior distribution, which is the left-hand side of Equation 3.7 by directly computing $P(\theta)$ and $P(D|\theta)$, and their product, for a very large ensemble of values of θ sampling strategically the n-dimensional space defined by the dimension of θ[29]. When applying MCMC sampling, a new parameter set (θ^{k+1}) is drawn from normal distributions with (θ^{k}), as the mean. Using the new parameter set, the posterior probability is calculated and compared to the previous set ($r = \frac{f^{k+1}}{f^{k}}$). With probability r greater than 1, the sample set is accepted, while with probability r less than 1, the sample set is rejected. Should the new parameter set be rejected, the previous parameter set ($\theta^{k+1} = \theta^{k}$) will be retained. We repeat this process for 1000 samples. Using these samples, we compute summary statistics on parameter posterior distributions.

3.3 Results and Discussion

3.3.1 National vs. Global Mercury Inventory

Figure 3-5 compares ASGM Hg emissions estimates from two different bottom-up inventories regrided to the GEOS-Chem 2×2.5 grid used in the simulations in this study. The GMA 2018 estimates of Hg emissions from ASGM activities in Peru for 2015 as distributed by Steenhuisen and Wilson[33] are shown in Figure 3-5,(a). Furthermore, Figure 3-5,(b) represents my interpretation of how the Peru ASGM Hg emissions estimates from the AGC's inventory[17] would be mapped on to the GEOS Chem Grid. The estimates for the total ASGM emissions from Peru are almost similar in both inventories, 110.4 t/y in the GMA 2018 and 108.74 t/y in the AGC national inventory.

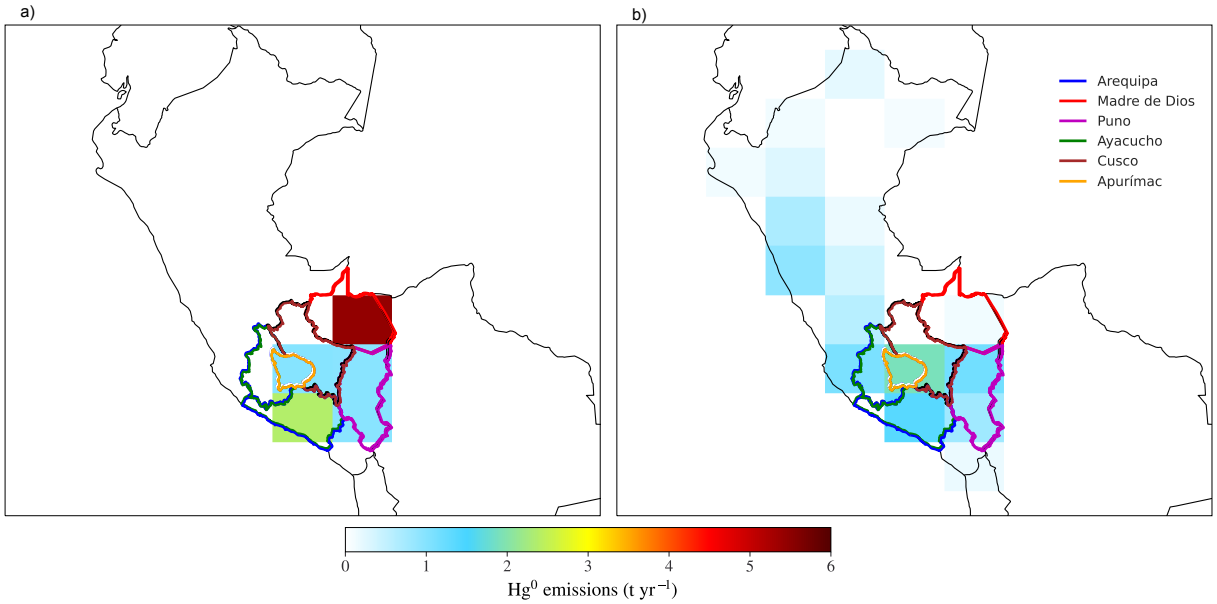

Figure 3-5: The AGC Peru National ASGM Hg emissions inventory as published in [17] and regridded to the GEOS-Chem 2×2.5 grid resolution is shown in (a).How the ASGM Hg emissions in Peru were distributed in two bottom-up inventories. The GMA2018 ASGM Hg emissions inventory for 2015 as distributed in Steenhuisen and Wilson [33] and regridded to the GEOS-Chem 2×2.5 grid resolution is shown in (b).

The AGC's Peru national inventory attributed most of the ASGM Hg emissions to the South Eastern departments in the country[17]. As seen in Table 3.2, the Madre de Dios department is the largest source of Hg emissions, followed by Arequipa, Puno, Ayacucho, Cusco, respectively. The rest of Peru together contributes about 0.98 tonnes of Hg emissions annually. In contrast with the AGC's method, Steenhuisen, and Wilson[33] based the Hg emissions spatial distribution on a proxy based on the likelihood of gold occurrence in soils, sediments, and bedrock and knowledge of actual ASGM activity. For Peru, they used the global alluvial gold map and a (gold) mining concessions dataset for Peru.

Table 3.2: Comparison of Peruvian ASGM Hg emissions estimates from the GMA2018 inventory for 2015 and estimates from the AGC national inventory of ASGM Hg emissions from the case study region. The emissions units are tons/year, and the right-most column shows the percentage difference between the AGC and GMA 2018 Hg emissions estimates.

Region	**AGC**	**GMA 2018**	**Percentage Difference**
	($t \cdot y^{-1}$)	($t \cdot y^{-1}$)	(%)
Madre de Dios	54.46	1.39	-97.45
Puno	19.37	19.42	+0.26
Arequipa	23.86	18.99	-20.41
Apurimac	0.03	19.32	+64300.00
Ayacucho	9.15	8.99	-1.75
Cusco	0.89	0.04	-95.50
Rest of Peru	0.98	42.25	+4211.22
Total	108.74	110.40	

The Madre de Dios department is a well-known ASGM hotbed in Peru, and within the Amazon region hence the GMA 2018 estimate of Hg emissions of 1.39 t/y can be easily identified as inaccurate. Moreover, Diringer et al.[47] estimated that the amount of Hg used in ASGM in Madre de Dios was at least 30 tons per year, which also undermines the GMA 2018 estimate.

As discussed in Chapter 2, the Base (ASGM = ON) simulation model did not reproduce atmospheric Hg concentrations, and the above comparison of global and national inventories was conducted to determine the role played by emission inputs in the poor model's replication of observed atmospheric concentrations. In light of the uncertainty in the inventories of Hg emission estimates and the above findings about the differences in the inventories, it was hypothesized that the poor predictions of Base (ASGM = ON) simulation may be the result of incorrect emission parameterization in GEOS-Chem . Following are the results of scaling the emissions from the departments in the case study and comparing them with observations. A top-down estimate of Hg emissions for Peru is also provided.

3.3.2 GEOS-Chem Predictions vs. Observations at Chalcataya

The comparison of the GEOS-Chem predicted Hg^0 concentration to observed TGM at CHC for the one year from 2014/07/03 to 2015/07/03 is shown in Table 3.3. The metrics being compared on the table are the mean (μ), standard deviation (σ), interquartile range (iqr), Spearman correlation (r_s) and Pearson correlation (r).The mean Hg^0 concentration produced by the No ASGM (ASGM = OFF) simulation was within 1% of the observed TGM concentration as seen in Table 3.3. On the contrary, the average Hg^0 produced by the Base (ASGM = ON) simulation overestimated the mean by 29%.

Table 3.3: Characteristics of observed and modeled Hg concentration in CHC where μ is the annual average Hg concentration, σ is the standard deviation, iqr is the interquartile range, r_s is the Spearman correlation, r is the Pearson correlation

	μ (ng m^{-3})/year)	σ (ng m^{-3})/year)	iqr (ng m^{-3})/year)		
Observations	0.90	0.16	0.18		
Simulations				r_s	r
No ASGM (ASGM=OFF)	0.91	0.060	0.11	0.17	0.14
Base (ASGM=ON)	1.2	0.14	0.20	0.12	0.27

Figure 3-6 shows a detailed comparison of the simulated Hg^0 concentration and the observed TGM concentration at CHC. The observations (in red) are plotted as a function of time in plots (a) and (c) with the No ASGM (ASGM = OFF) simulation (in green) in plot (a) and the Base (ASGM = ON) simulation in (blue) in plot (c). The low correlation between both modeled Hg^0 concentrations and the observations is also evident in the scatter plots in (b) and (d). However, the Base (ASGM = ON) simulation closely approximates the variability (defined by the standard deviation) in the observed Hg concentration as its standard deviation is only 12.5% less than the observation standard deviation, yet the No ASGM (ASGM = OFF) simulation standard deviation is 62.5 % less than the observation standard deviation. While here, the dataset has been truncated to one year from 2014/07/03 to 2015/07/03, this study follows Chapter 2, where the entire CHC dataset was compared with the modeled Hg^0 concentration at CHC.

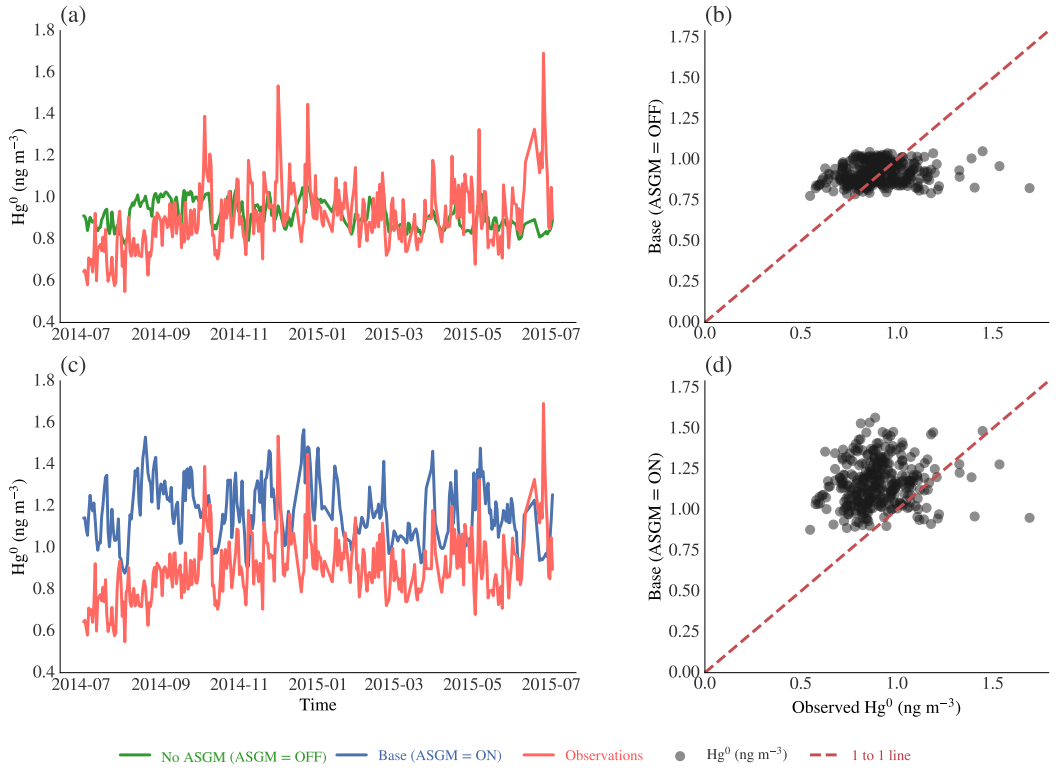

Figure 3-6: The observations (in red) are plotted as a function of time in plots (a) and (c) with the No ASGM (ASGM = OFF) simulation (in green) in the plot (a) and the Base (ASGM = ON) simulation in (blue) in the plot (c). Analysis of the observed Hg concentrations vs. the No ASGM (ASGM = OFF) simulation shows how the modeled mean closely approximates the observed mean and poorly estimates the daily variability, as shown by the difference in the size of the daily spikes of the Hg concentrations. The scatter plots in (b) and (d) represent the modeled Hg^0 as a function of the measured TGM concentration.

Even though GEOS-Chem closely approximated the mean Hg concentrations at CHC in the No ASGM (ASGM = OFF) simulation , the Spearman (r_s) and Pearson (r) correlations between the modeled and observed concentrations were very low at 0.17 and 0.144, respectively. Moreover, the coefficient of determination, R^2 between the observed and modeled concentrations in No ASGM (ASGM = OFF) simulation case was almost zero at 0.0207. This is in line with the general result in Chapter 2 that the model poorly estimates the observed Hg emission concentrations in the atmosphere. Brasseur and Jacob (p.471)[29] argue that in cases where a model captures the observed means but not the observed variability, the mean may be wrongly interpreted [29]. In line with Brasseur and Jacob's argument, the wrong interpretation of the No ASGM (ASGM = OFF) simulation mean is encapsulated in the direct comparison of the No ASGM (ASGM = OFF) simulation and the TGM concentration at CHC . This is because Hg concentrations in the atmosphere captured in the TGM concentration at CHC are affected by ASGM emissions near

CHC. Moreover, a poor definition of dry deposition or vegetation uptake in the model further leads to underestimating observed Hg concentrations.

The Base (ASGM = ON) simulation reproduces the iqr and 95th % confidence interval better than it reproduces the mean, as seen in Figure 3-8. Density plots of the modeled and observed Hg concentration at Chalcataya are shown in Figure 3-8. In (a), the actual distributions for the two simulations and the observations are plotted where the observed TGM concentration distribution is shown in red, the distribution of the Hg^0 concentration predicted by the No ASGM (ASGM = OFF) simulation is shown in green, and that produced by the Base (ASGM = ON) simulation is shown in blue. Figure 3-8 (b) shows the identical distributions to (a) after standardization by subtracting the mean in each distribution to see how the shapes of the distributions compare with each other.

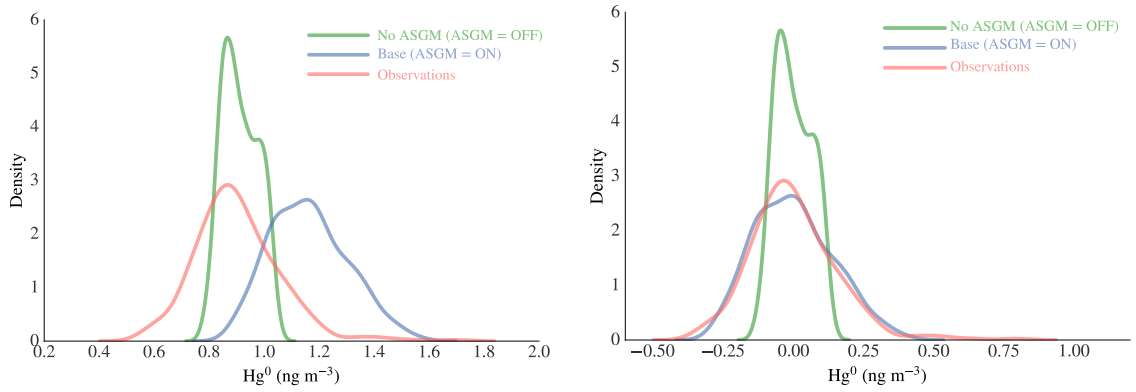

(a) (b)

Figure 3-8: Density plots of the modeled and observed Hg concentration at Chalcataya. In (a), the actual distributions for the two simulations and the observations are plotted where the observed TGM concentration distribution is shown in red, the distribution of the Hg^0 concentration predicted by the No ASGM (ASGM = OFF) simulation is shown in green, and that produced by the Base (ASGM = ON) simulation is shown in blue. In (b), the same distributions are shown after standardization by subtracting the mean in each distribution for easy comparison of the shapes of the distributions

Figure 3-8, b) shows how the Hg^0 concentration produced by the Base (ASGM = ON) simulation have a distribution that is similar to the distribution of the observations in terms of standard deviation, iqr and 95^{th} percentile range . The No ASGM (ASGM = OFF) simulation produced the modeled Hg^0 concentration at CHC shows no instance of high Hg^0 concentrations at CHC, and the high concentrations are only produced by the Base (ASGM = ON) simulation . These density

plots inform us that ASGM emissions primarily influence the range of observed Hg concentrations in the atmosphere at CHC. Consequently, metrics such as the standard deviation, iqr , and 95^{th} percentile range may lead to more informative comparisons between the modeled Hg^0 concentration at CHC and the TGM concentration at CHC than the mean.

3.3.3 Comparison of Observations with Emission Modification

The sensitivity of the modeled Hg^0 concentration at CHC to the changes in Hg emissions from each grid box in the case study region was investigated by finding the mean, iqr , and correlation between the modeled Hg^0 concentration at CHC and the TGM concentration at CHC as functions of the emissions from each specific grid box. Each plot in Figure 3-9 shows the relationship between the mean of the modeled Hg^0 concentration at CHC as a function of Hg emissions from the grid box corresponding to the respective region in the case study. For each plot, the emissions from one grid box are varied between 0 to 100 tons in increments of 10 tons, while the emissions from the other grid boxes are kept at their Base (ASGM = ON) simulation level.

The means of the modeled Hg^0 concentration at CHC for a given amount of Hg emissions from each grid box are compared to the red horizontal line. This red horizontal line indicates the value of the mean of the TGM concentration at CHC (0.90), as presented in Table 3.3. Moreover, the blue dashed line shows the linear regression line for the values of the modeled Hg^0 concentration at CHC as a function of the Hg emissions. All the plots show that the mean of the Hg concentration changes linearly with an increase in emissions and have a R^2 value of 1, which validates the linear assumption between emissions and concentrations. Furthermore, none of the blue dashed lines intersect the red line within the given emissions range, which also undermines the mean as a metric for comparing the modeled Hg^0 concentration at CHC to the TGM concentration at CHC .

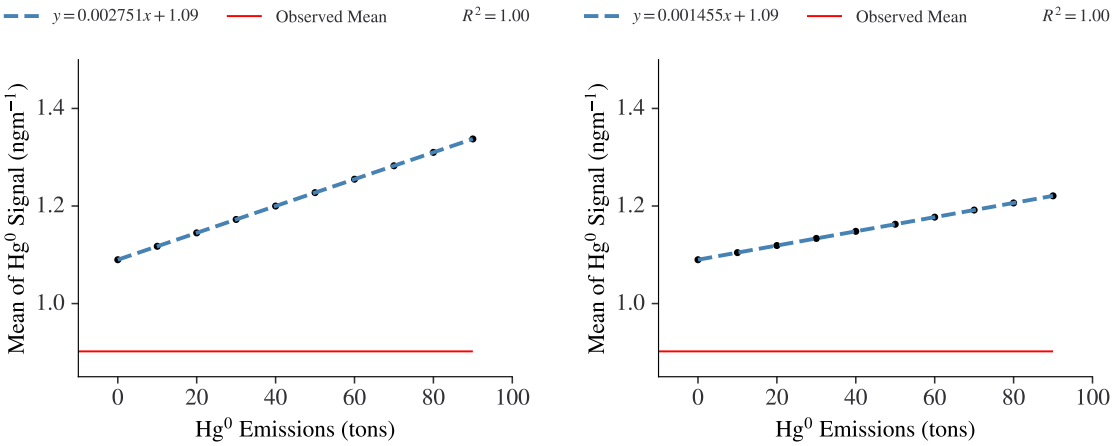

(a) South Puno

(b) North Puno

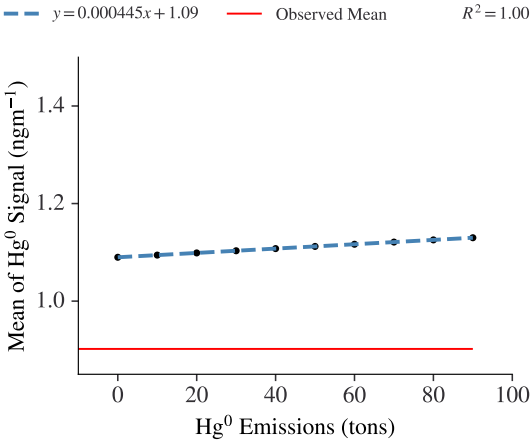

(c) Arequipa

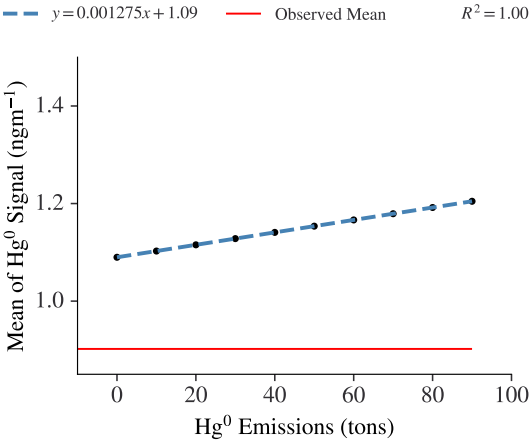

(d) Apurimac

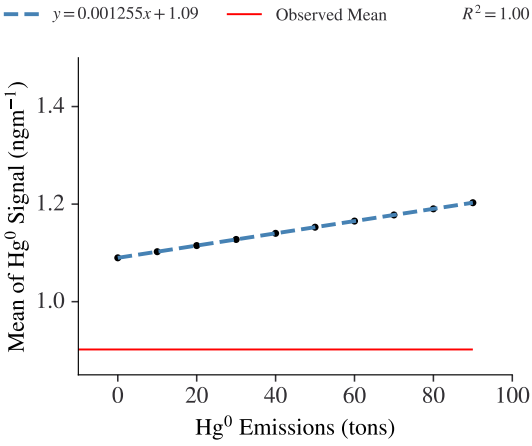

(e) Madre de Dios

Regression of mean of modeled atmospheric Hg^0 concentration at CHC as a function of the emissions from the respective grid boxes in the case study region. The red horizontal line indicates the value of the mean TGM concentration at CHC, 0.90. The dashed blue line indicates the linear regression line on the means of concentrations at CHC for different emission amounts from the respective regions.

Figure 3-9

Contrary to Figure 3-9 where the relationships between the Hg emissions and the mean of the modeled Hg^0 concentration at CHC have similar R^2 values (R^2 =1), the relationship between the iqr of the modeled Hg^0 concentration at CHC and the emissions from each grid box in Figure 3-10 have different R^2 values. For each plot in Figure 3-10, the emissions from one grid box are varied between 0 to 100 tons in increments of 10 tons while the emissions from the other grid boxes are kept at their Base (ASGM = ON) simulation level. Even though the R^2 values are different, they are all above 0.85, which validates the linear assumption between the emissions and the R^2 values of the Hg concentration. The values of the iqr for a given amount of Hg emissions from each grid box are compared to the red horizontal line, which indicates the iqr of the TGM concentration at CHC , (0.16) .

All the lines showing the relationship between the iqr of the modeled Hg^0 concentration at CHC and the emissions intersect the red line representing the iqr of the TGM concentration at CHC . The Hg emissions value of the point of intersection between the regression line and the red line can be interpreted as what the emissions from the given grid box should be for the the modeled Hg^0 concentration at CHC to match the the TGM concentration at CHC . The actual values of the emissions can also be calculated using the regression equation given on each plot.

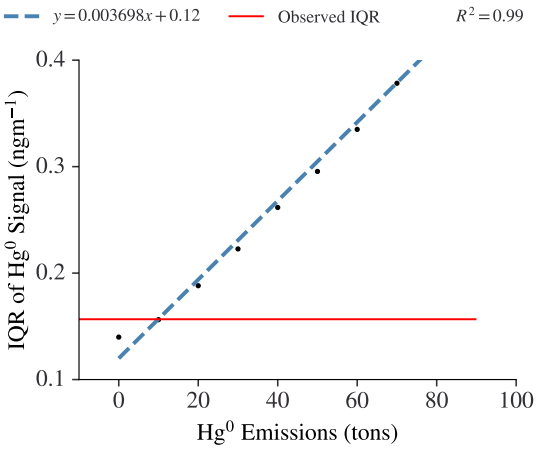

(a) South Puno

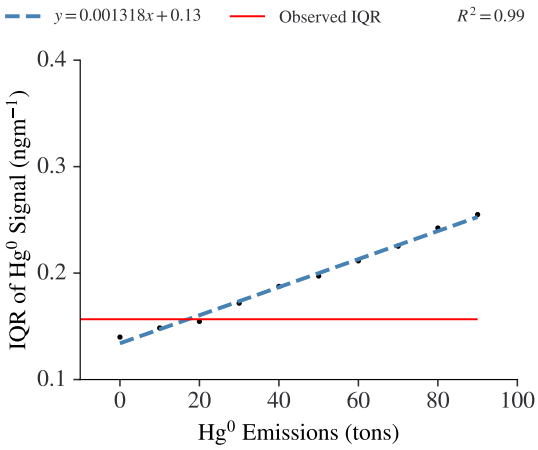

(b) North Puno

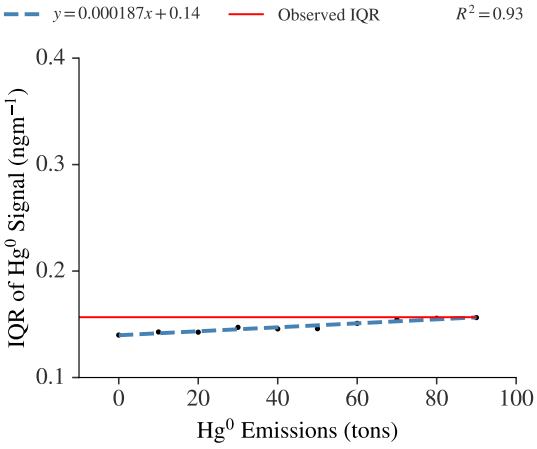

(c) Arequipa

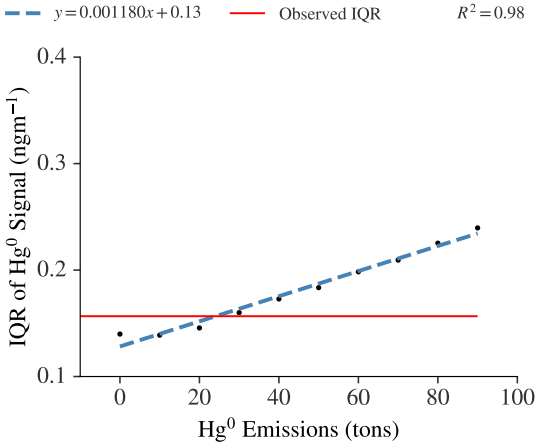

(d) Apurimac

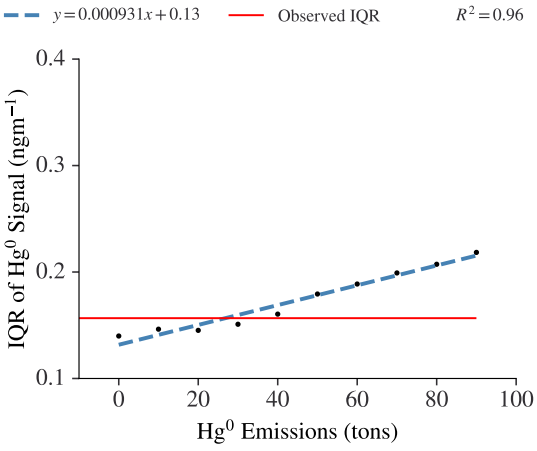

(e) Madre de Dios

Regression of IQR of modeled atmospheric Hg^0 concentration at CHC as a function of the emissions from the respective grid boxes in the case study region. The red horizontal line indicates the value of the IQR of the f TGM concentration at CHC, 0.16. The dashed blue line indicates the linear regression line on the IQRs of concentration at CHC for different emission amounts from the respective regions.

Figure 3-10

Unlike in Figures 3-9 and 3-10, the Pearson correlation coefficient (r) between the TGM concentration and the modeled Hg^0 concentration at CHC has a negative trend in all the emissions scenarios. Int he concentxt of model obsevation comparison, the Pearson correlation coefficient characterizes how patterns in the observations are matched by patterns in the model[29]. According to Brasseur and Jacob, values of r near zero imply that the variability in the observations is controlled by processes that the model does not capture. Table 3.3 shows that r of the Base (ASGM = ON) simulation is very low at 0.27. As in Figures 3-9 and 3-10, the emissions from the corresponding region are varied from 0 to 100 tons in increments of 10 tons for each plot in Figure 3-11.

For each emissions scenario, the correlation between the TGM concentration and the modeled Hg^0 concentration at CHC is indicated by the black dot. The red horizontal line indicates the Pearson correlation between the TGM concentration at CHC and the Base (ASGM = ON) simulation (0.27). The dashed blue line shows the regression line of the correlation between the modeled Hg^0 concentration at CHC and the TGM concentration at CHC as emissions from each grid box increase. It is evident that increasing the emissions from one region while keeping the emissions from other regions at the Base (ASGM = ON) simulation level did not lead to improvements to the extent to which the patterns in the observations are matched by the pattern in the modeled Hg^0 concentration at CHC . However, the rate at which the correlation decreases may reveal information about the sensitivity of the modeled Hg^0 concentration at CHC to the emissions from a specific region. For instance the shallow slope in the regression line for the Madre de Dios scenarios may be an indicator that the emissions from Madre de Dios are underestimated.

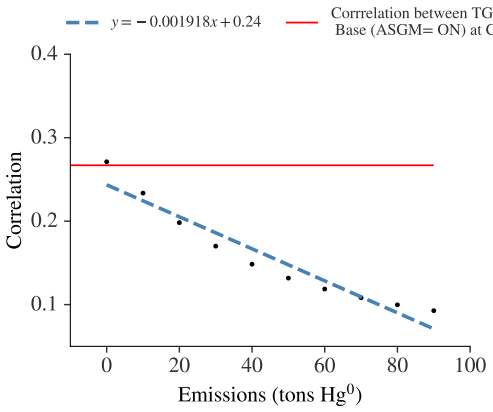

(a) South Puno

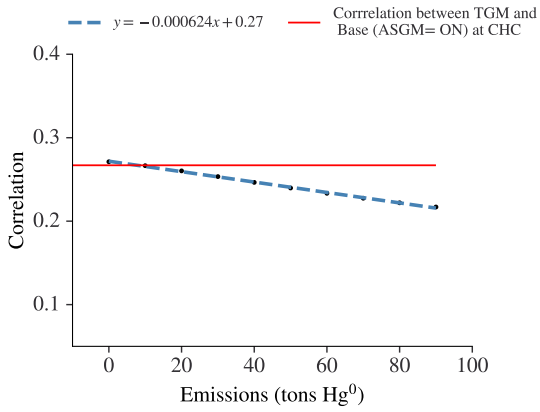

(b) North Puno

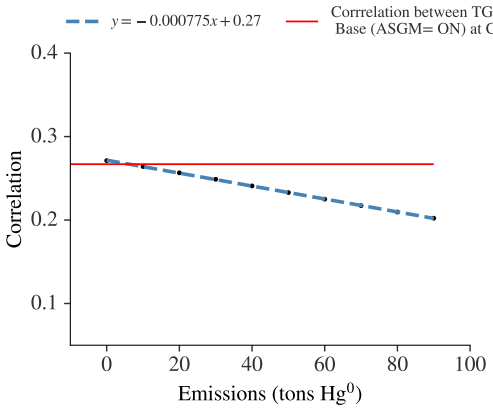

(c) Arequipa

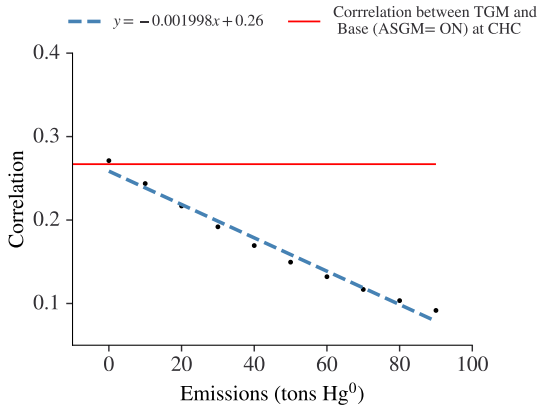

(d) Apurimac

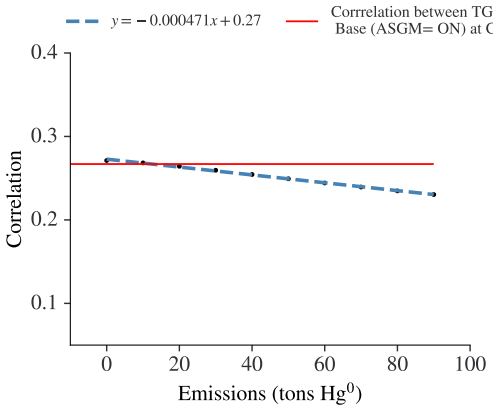

(e) Madre de Dios

Regression of correlation between the TGM concentration and modeled atmospheric Hg^0 concentration at CHC as a function of the emissions from the respective regions. The red horizontal line in each plot indicates the value of the correlation between the TGM concentration and Base (ASGM = OFF) modeled Hg^0 concentration at CHC The dashed blue line indicates the linear regression line on the correlation between the TGM concentration at CHC and the modeled Hg0 produces by different emission amounts from the respective regions.

Figure 3-11

This section has shown the effect of changing Hg emissions from individual grid boxes in the modeled Hg^0 concentration at a distant active monitoring site like CHC. ASGM Hg emissions estimates of the from the different regions would be obtained graphically from each of the plots by identifying the point of intersection between the red horizontal line and the regressions line or solving the regression line equation. However, the range of these estimates would not be robust; hence following section presents the emission estimates generated using the MCMC, which accounts for emission changes from multiple regions.

3.3.4 Estimating Emissions with Markov Chain Monte Carlo

Based on the 95^{th} percentile range , the MCMC approach produced Hg^0 emissions estimates within the range of bottom-up inventory estimates. The distributions of the estimates produced by the MCMC approach are shown in Figure 3-12. The box and whisker plots illustrate Hg0 emissions when the 95th percentile range is used to compare the modeled Hg0 concentration and the TGM concentration. In the box plots, the horizontal lines represent the emission estimates based on bottom-up inventories. Solid horizontal lines represent emission estimates from the GMA 2018 inventory [3, 33]; dashed lines represent emission estimates from Peru's bottom-up inventory. In Table 3.4, we describe the mean estimates of emissions from these regions and their ranges [17].

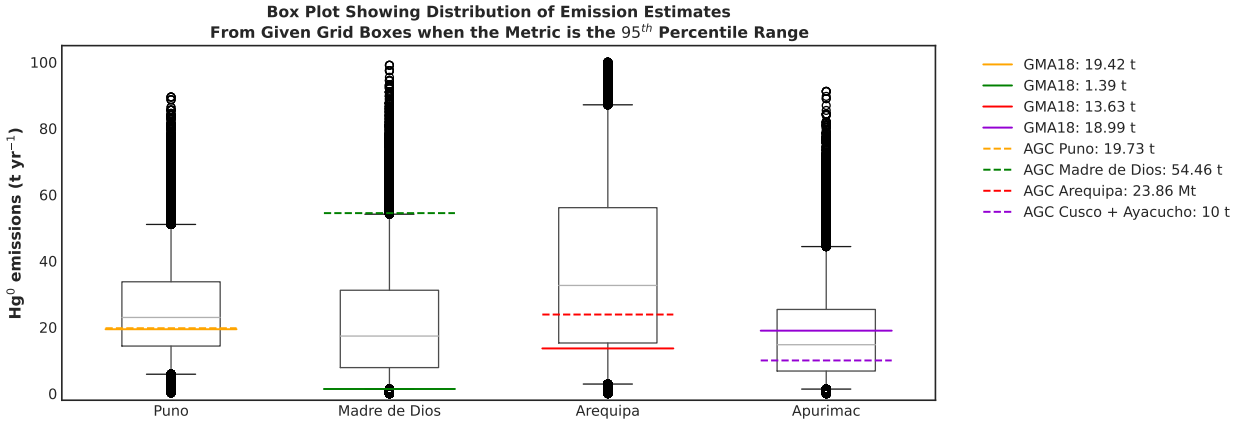

Figure 3-12: Emission Estimates when the 95^{th} percentile range is used as the metric to compare the model outputs to observations. The horizontal lines representing the emission estimates from the bottom-up inventories are traced over the box plots. The solid horizontal lines represent the emission estimates from the GMA 2018 inventory [3, 33] and the dashed lines represent the emission estimates from the bottom-up inventory published by the Artisanal Gold Council[17].

These are the first ever top-down estimates of Hg emissions from ASGM activities. Even though

the ranges of the estimates are wide, they result from the uncertainty in the models and data we could access. Therefore, these results may be improved if more data from monitoring sites were available to constrain the emissions. Nevertheless, the top-down estimate of the total amount of ASGM Hg emissions under-predicts the GMA 2018 total estimate for Peru by a factor of 1.09 and the AGC estimate by a factor of 1.08. The comparison of the top-down ASGM Hg estimates with the bottom-up estimates is visualized in Figure 3-13. It is essential to highlight the Madre de Dios region's estimate of 21 tons/year of ASGM Hg emissions. This estimate is an improvement aligned with the literature about the high ASGM Hg emissions in the region. However, it is still a drastic underestimate compared to the AGC baseline ASGM Hg estimate for Madre de Dios.

Table 3.4: Table showing the emission estimates for each of the grid boxes in the case study region when the 95^{th} percentile range is used as the metric to compare the model outputs to observations

Region	**Emission Estimate (Mg)**	**Range of Estimate (Mg)**
Madre de Dios	21	$1.36 - 54.12$
Apurimac	17	$1.36 - 44.37$
Arequipa	37	$2.88 - 87.14$
Puno	25	$5.85 - 51.05$
Total	101	$11.45 - 236.69$

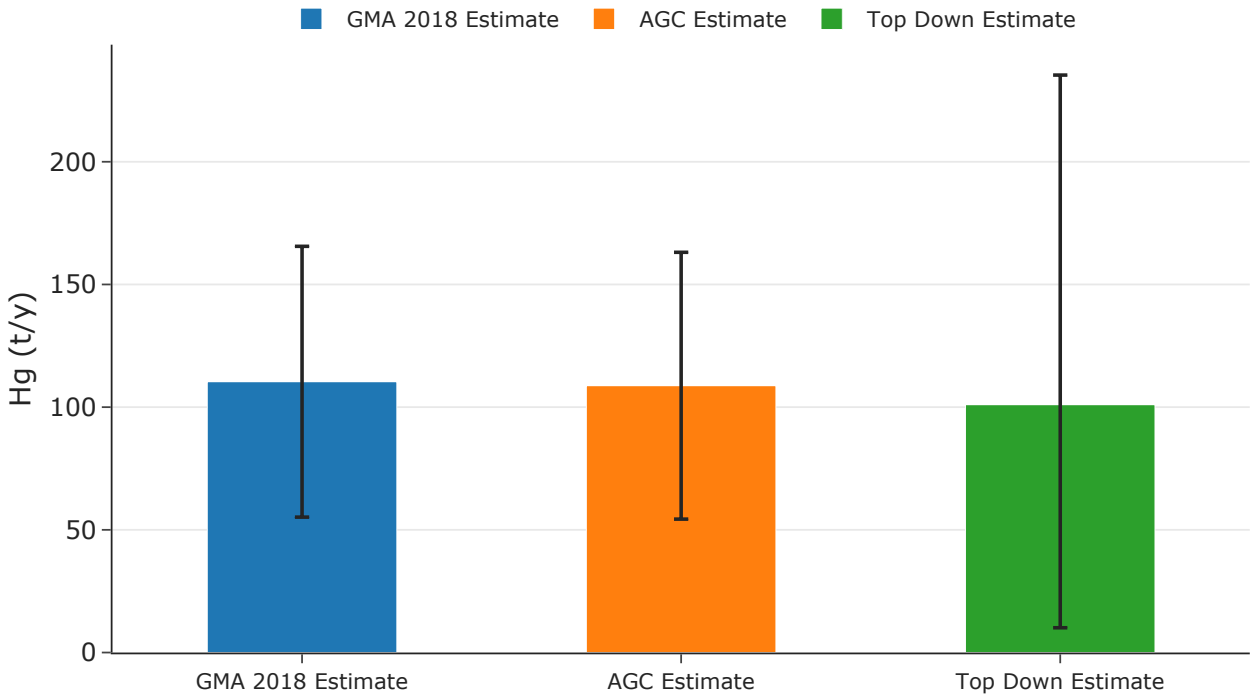

Figure 3-13: Bar chart shows the different estimates of the total ASGM Hg emissions from Peru. The height of the bars indicates the estimated Total emissions, and the error in each estimate is shown by the error bars.

Our study produced top-down estimates of ASGM Hg emissions for four Peruvian departments and thus the country's total ASGM Hg emissions estimates. Table 3.4 shows Peru emits 101.23 tons of Hg annually, ranging from 11.45 tons to 236.69 tons. There is a wide range here, but it is a confidence interval based on the data and the uncertainty of the model discussed so far. The estimates would be improved if more relevant measurements of atmospheric Hg were used instead of just one-site data. Another potential source of refinement in the estimates may result from the model's improved parameterization of vegetation uptake discussed in Feinberg et al [35].

Model improvements and more time series atmospheric Hg concentration data may enable us to use the mean as another constraint for producing Hg^0 emission estimates. Also, these results demonstrate that extreme values are vital for quantifying non-point sources like ASGM, where variability over time is somewhat unpredictable. The analysis in this chapter focused on a region in Peru where ASGM dominates. These top-down will be challenging to implement in areas where ASGM co-occurs with many point sources, such as Southeast Asia, where biomass and coal are burned simultaneously. Furthermore, the global resolution of GEOS-Chem is not particularly suitable for monitoring Hg in mountainous regions such as CHC. Future work may

extend this method and this proof of concept using more satisfactory results focusing on the region.

In addition to helping resolve the differences in global and national ASGM Hg emission estimates, the above analysis also provides a stronger foundation for answering the second question about how regional monitoring networks can improve the utility of models for MC effectiveness evaluations. Creating these inverse models for PAS data would be challenging since it is a discrete dataset that only shows averages for a specific period. However, active sampling data is continuous and can be analyzed through summary statistics such as mean, iqr , correlation, and 95^{th} percentile range . Even though the mean of the concentrations was not viable for this analysis, the other metrics were instrumental in generating the results.

3.4 Conclusion

The study showed that time series monitoring data and the GEOS-Chem CTM could be used together to produce top-down estimates of Hg emissions from ASGM activities. In spite of limited data sources and uncertain models, our ASGM Hg emission estimates were within ranges estimated by GMA 2018 [3, 33] and AGC [17]. The objective of this study was to prove the concept of top-down techniques for estimating Hg emissions from ASGM activities. In addition to improvements in the model, more time series data would help reduce the uncertainty in this approach and potentially make mean concentrations more useful. We applied the top-down techniques to a country in Latin America, where ASGM is the dominant source of pollution. For future research and interest in applying it elsewhere, it is essential to note that extending this approach to areas where ASGM Hg emissions occur alongside other sources may prove challenging.

Chapter 4

Policy Recommendations and Conclusions

Quantitative estimates of Hg emitted into the atmosphere by each country and the corresponding impacts on human health and the environment are crucial for effectively assessing whether legally-binding agreements such as the Minamata Convention (MC) are effective. In such a context, it is evident that quantifying current and future emissions with the best degree of accuracy is an indispensable prerequisite. Consequently, developing and using appropriate methodologies and tools for calculating current emissions and projections within a reasonable uncertainty range is crucial. This chapter aims to provide recommendations on using atmospheric models and monitoring to policymakers in regions with high ASGM incidence to understand ASGM Hg emissions to the atmosphere and its evolution over time.

Section 4.1 gives a quick summary of the first three chapters. Section 4.2 discusses the discrepancies between GMA 2018 ASGM Hg emission estimates and those in the NAPs. This section aims to underscore the value add that atmospheric monitoring and modeling provide in the presence of such inconsistencies. Moreover, section 4.3 uses the Montreal Protocol as an example to discuss the possibilities provided by combining atmospheric monitoring and modeling to inform actions by parties as well as evaluate the effectiveness of the MC. The discussion in this section drives the point that atmospheric monitoring and modeling provides valuable information but may be politically controversial depending on the expectation of parties and the type of penalties imposed on violators of MC's legally binding agreements. Next, section 4.4 discusses recommendations for governments and policymakers by

emphasizing that governments need to prioritize atmospheric monitoring and modeling to understand and combat ASGM Hg emission sources.

4.1 Review of First Three Chapters

This chapter builds upon the results of the first three chapters of this thesis. Chapter one discussed the nature of ASGM activities and their estimated contribution to the global Hg budget. Moreover, challenges regarding knowledge of ASGM Hg emissions were discussed, including the vast uncertainties in ASGM Hg emission estimates. This thesis was partly motivated by the lack of sufficient atmospheric monitoring in most regions where ASGM is prevalent and the absence of modeling studies evaluating Hg emissions from regions with high ASGM emissions. Furthermore, Chapters 2 and 3 showed how data from different Hg atmospheric concentration monitoring technologies could be leveraged and integrated with the GEOS-Chem CTM results to investigate ASGM Hg pollution. Chapter 2 compared the temporal and spatial characteristics of observed and modeled atmospheric Hg concentrations. PAS GEM measurements provided helpful information about the distribution of Hg concentrations across Latin America. Additionally, it was discussed that a network of PAS provides high-quality data while being accessible and affordable to deploy. However, PAS is limited because it does not provide continuous data about atmospheric Hg concentrations. On the other hand, active sampling techniques such as those conducted by the GMOS Network provided valuable time series data about the atmospheric Hg concentrations. These data enabled broader analysis through the utilization of more metrics to evaluate Hg emissions and better understand temporal variations of Hg concentrations in the atmosphere. By combining active monitoring stations with models, it may be possible to improve understanding of mercury levels in the atmosphere and better define source-receptor relationships.

4.2 Discrepancies Between Global and National ASGM Mercury Estimates

According to Evers et al.[20], country-specific actions under Article 7 of the MC will differ from country to country, and this variability poses a challenge to assessing the MC's effectiveness.

Additionally, they argue that understanding changes in the overall use of Hg in the global ASGM sector can be informed by tracking progress in individual countries. They suggest a compilation, visualization, and mapping of the respective data to track this progress across ASGM countries. The value added by baseline estimates of emissions to policy making is also recognized in the MC's paragraph 3 of Article 7, which stipulates that each party that notifies the secretariat that (ASGM) and processing in its territory is more than insignificant shall develop and implement a national action plan (NAP) per annex C to the MC. In addition, annex C (d) states that the NAP shall include baseline estimates of the quantities of Hg used and the practices employed in ASGM and processing. As of this writing, 18 countries have submitted their respective NAPs. The estimates of how much Hg is used in their territories are shown in Figure4-1, which is a bar chart comparing the estimates of annual average Hg emissions predicted in the GMA 2018 inventory in light blue vs. annual average Hg emissions baseline estimates (shown in dark blue) that were reported by the respective countries in their NAPs [3].

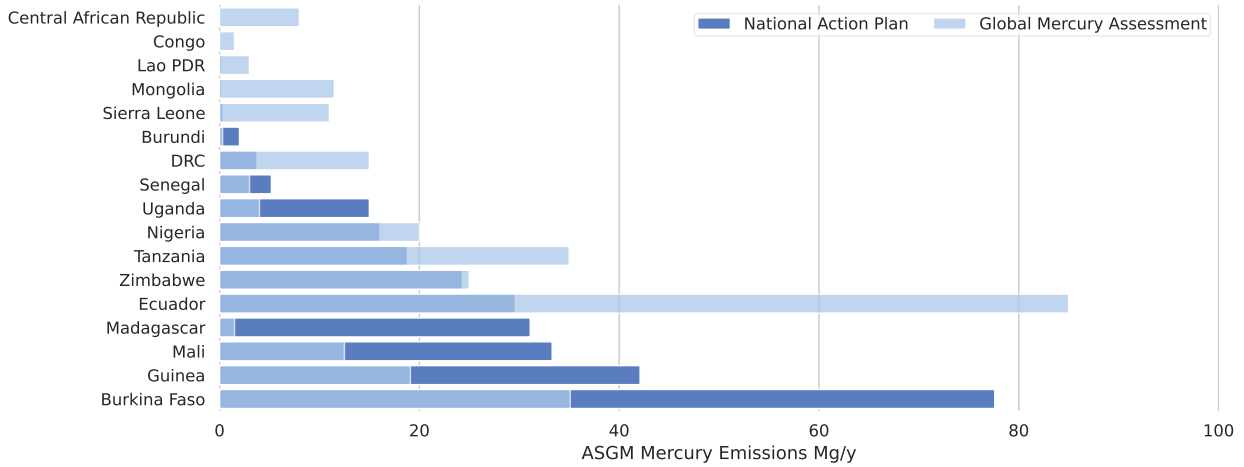

Figure 4-1: Bar chart comparing the estimates of annual average Hg emissions predicted in the GMA 2018 inventory in light blue vs. annual average Hg emissions baseline estimates (shown in dark blue) that were reported by the respective countries in their NAPs [3]

In Figure 4-1, it is evident that the difference between the global estimates and the NAP estimates is vast for some countries. While the baseline estimates of Hg use in ASGM as reported in the NAPs and global inventories are critical, data from monitoring networks combined with atmospheric models provide additional tools to evaluate the changes in Hg in the atmosphere. The differences in the estimates do not necessarily indicate emission increases, but they reflect the uncertainties in the global emission estimates.

4.3 Informing the Use of Atmospheric Modeling for Quantifying ASGM Emissions in the Minamata Convention through Experiences from the Montreal Protocol

Monitoring atmospheric concentrations of pollutants of interest and using atmospheric models to understand the data has been critical in evaluating global legally-binding environmental agreements such as the Montreal Protocol. For instance, Rigby et al. 2019 showed how vital the combination of atmospheric monitoring networks and modeling is when they quantified the amount of an observed increase in CFC-11 and identified where the source was located[48]. They used high-frequency atmospheric observations from Gosan, South Korea, and Hateruma, Japan, and global monitoring data and atmospheric CTM simulations to investigate regional CFC-11 emissions from eastern Asia.

The above example about the Montreal protocol showcases the multiple benefits of atmospheric monitoring and modeling. For instance, Rigby et al.[48] showed that emissions from eastern mainland China were 7.0 ± 3.0 (±1 standard deviation) gigagrams per year higher in 2014–2017 than in 2008–2012 and that the increase in emissions arose primarily around the northeastern provinces of Shandong and Hebei[48]. This kind of precision of emission estimates and the approximate location of their sources would be beneficial for evaluating the effectiveness of MC efforts aimed at reducing Hg emissions. Policymakers would value such information because it would give them precise data about the amounts of emissions and where they should look for the sources. However, it is uncertain if this level of precision could be achieved for an emission source like ASGM, given that it is not a point source.
Another critical aspect of the information provided by the approach discussed in this thesis is the ability to determine areas that have a low likelihood of being sources of increase in emissions. This benefit was also demonstrated by Rigby et al. (2019) in that they could conclude that there was no evidence for a significant rise in CFC-11 emissions from any other eastern Asian countries or other regions of the world where there are available data for the detection of regional emissions.

A look at China's response to scientific information about its increased CFC emissions in the Montreal Protocol example above may provide insight into possible answers by parties when

they are notified about emission violations within their territory. China questioned the conclusions of the scientific study noting significant uncertainty. However, they also acknowledged the importance of atmospheric monitoring. They developed a plan to establish a national monitoring network, including substantial penalties for companies that produce insulation foam for ozone-depleting chemicals illegally. Considering that ASGM occurs mainly in poor communities in countries in the global south, the Minamata Convention may need to develop a different strategy for helping countries respond to sudden increases in their ASGM emission sources. For instance, PAS technologies could be deployed at locations of interest once regional active monitoring networks and models have identified spikes in ASGM Hg emissions. Lawmakers should rely on legal measures to curb emissions, such as banning mercury or restricting ASGM communities as a last resort. These command-and-control strategies have been shown to dissuade miners from cooperating[49, 50].

4.4 Recommendations

As part of monitoring ASGM activities and defining policy related to ASGM activities, government officials and policymakers are encouraged to include atmospheric monitoring. Governments may be able to set up monitoring within their territories by using PAS technologies. Moreover, governments are encouraged to establish regional active monitoring stations in collaboration at the regional level. According to chapter three, a reasonable estimation of emissions can be made based on data from one station. In this way, a few regional active monitoring networks and widespread national PAS networks may prove helpful for evaluating the effectiveness of MC activities.

The monitoring of atmospheric Hg can provide information about ASGM activities and help identify them. As a result, these data can be used to establish a baseline of mercury use in ASGM and to evaluate policies related to reducing it. Through cartographic and statistical products, monitoring and modeling outputs can be understandable to non-technical audiences, thus facilitating artisanal mining policy development.

Modeling the atmosphere using CTMs requires technical skills not usually available in government agencies or policy agencies because it requires technical competencies typically found in scientific communities. Consequently, investing in capacity building among mining administrations lacking technical knowledge and soliciting researchers' know-how from local universities are critical

recommendations for government officials and policymakers.

It is necessary to consider that technical competency is not always present in local communities and mining associations. As a result, their involvement in monitoring programs and policy development may be reduced or compromised. Tensions can sometimes be exacerbated by this, which undermines local trust. Therefore, government officials and policymakers should include local communities and artisanal miners when developing ASGM policies and programs.

4.5 Conclusion

Chapter four built upon the findings of the previous three chapters. We referenced one of this thesis's primary motivations, detailed in chapter one, where we discussed the nature of ASGM activities and their estimated contribution to the global Hg budget. We also highlighted chapters 2 and 3 of this thesis, which addressed the first two questions by demonstrating how data from different technologies for monitoring Hg concentrations in the atmosphere can be leveraged and integrated with the GEOS-Chem CTM outputs to investigate Hg pollution from ASGM activities. Moreover, we showed that combining active monitoring stations with models may improve understanding of mercury levels in the atmosphere and better define source-receptor relationships. By comparing the GMA 2018 estimates with the NAP estimates provided by countries, we proposed that atmospheric monitoring and modeling can provide additional constraints on emissions sources in policy-making.

Furthermore, the Montreal Protocol was cited as an example of how atmospheric monitoring and modeling are valuable in effective policy-making and ensuring that parties take responsibility for violations of treaty obligations. However, it may be politically controversial depending on how parties perceive it. Lastly, we suggested countries engage in regional active monitoring that uses both PAS and active tracking, referring to the third chapter of this thesis, where we analyzed active monitoring data to produce the first top-down estimates of ASGM mercury pollution.

Bibliography

[1] Herman Gibb and Keri Grace O'Leary. Mercury Exposure and Health Impacts among Individuals in the Artisanal and Small-Scale Gold Mining Community: A Comprehensive Review. *Environmental Health Perspectives*, 122(7):667–672, July 2014.

[2] Louisa J. Esdaile and Justin M. Chalker. The Mercury Problem in Artisanal and Small-Scale Gold Mining. *Chemistry (Weinheim an der Bergstrasse, Germany)*, 24(27):6905–6916, May 2018.

[3] Arctic Monitoring and Assessment Programme United Nations Environment Programme. Technical Background Report to the Global Mercury Assessment 2018 [Pre-print]. 2019.

[4] planetGOLD. planetGOLD 2019/2020 Progress Report. Technical report, 2021.

[5] USAID. USAID. 2020. Case Study ASM and ASGM in Madre de Dios.pdf, October 2020.

[6] United Nations Environment Program UNEP. Minamata convention on mercury: text and annexes. 2013. Accepted: 2016-10-11T20:05:58Z Publisher: UNEP.

[7] United Nations Environment Programme. Reducing Mercury Use in Artisanal and Small-Scale Gold Mining: A Practical Guide. June 2012. Publisher: United Nations Environment Programme.

[8] United Nations Environment Programme. Developing Baseline Estimates of Mercury Use in Artisanal and Small-Scale Gold Mining Communities: A Practical Guide. 2015.

[9] United Nations Environment Programme UNEP and Global Mercury Partnership GMP. Developing a National Action Plan to Reduce and, Where Feasible, Eliminate Mercury Use in Artisanal and Small-Scale Gold Mining - Guidance Document. 2017. Accepted: 2018-05-28T08:40:50Z.

[10] UNEP. Guidance on monitoring mercury and mercury compounds to support the effectiveness evaluation of the Minamata Convention | Minamata Convention on Mercury. Technical report, September 2021.

[11] Akihiro Yoshimura, Koyo Suemasu, and Marcello M. Veiga. Estimation of Mercury Losses and Gold Production by Artisanal and Small-Scale Gold Mining (ASGM). *Journal of Sustainable Metallurgy*, 7(3):1045–1059, September 2021.

[12] United Nations Environment Programme UNEP. *Global Mercury: Supply, Trade and Demand.* September 2017. Accepted: 2017-09-14T06:26:20Z.

[13] Barbara Fraser. Peruvian Gold Rush Threatens Health and the Environment. *Environmental Science & Technology*, 43(19):7162–7164, October 2009. Publisher: American Chemical Society.

[14] Jennifer J. Swenson, Catherine E. Carter, Jean-Christophe Domec, and Cesar I. Delgado. Gold Mining in the Peruvian Amazon: Global Prices, Deforestation, and Mercury Imports. *PLOS ONE*, 6(4):e18875, April 2011. Publisher: Public Library of Science.

[15] Marcello M. Veiga, Peter A. Maxson, and Lars D. Hylander. Origin and consumption of mercury in small-scale gold mining. *Journal of Cleaner Production*, 14(3):436–447, January 2006.

[16] Sarah E. Diringer, Beth J. Feingold, Ernesto J. Ortiz, John A. Gallis, Julio M. Araújo-Flores, Axel Berky, William K. Y. Pan, and Heileen Hsu-Kim. River transport of mercury from artisanal and small-scale gold mining and risks for dietary mercury exposure in Madre de Dios, Peru. *Environmental Science. Processes & Impacts*, 17(2):478–487, February 2015.

[17] Artisanal Gold Council AGC. REPORTE DE INVENTARIO: Estimaciones De Referencia Del Uso Y Consumo De Mercurio En La Mineria De Oro Artesanal Y De Pequeña Escala En Perú. REPORTE DE INVENTARIO, Artisanal Gold Council, 2017.

[18] Katy Ashe. Elevated Mercury Concentrations in Humans of Madre de Dios, Peru. *PLoS ONE*, 7(3):e33305, March 2012.

[19] Francesca Sprovieri, Nicola Pirrone, Mariantonia Bencardino, Francesco D'Amore, Francesco Carbone, Sergio Cinnirella, Valentino Mannarino, Matthew Landis, Ralf Ebinghaus, Andreas Weigelt, Ernst-Günther Brunke, Casper Labuschagne, Lynwill Martin, John Munthe, Ingvar Wängberg, Paulo Artaxo, Fernando Morais, Henrique de Melo Jorge Barbosa, Joel Brito, Warren Cairns, Carlo Barbante, María del Carmen Diéguez, Patricia Elizabeth Garcia, Aurélien Dommergue, Helene Angot, Olivier Magand, Henrik Skov, Milena Horvat, Jože Kotnik, Katie Alana Read, Luis Mendes Neves, Bernd Manfred Gawlik, Fabrizio Sena, Nikolay Mashyanov, Vladimir Obolkin, Dennis Wip, Xin Bin Feng, Hui Zhang, Xuewu Fu, Ramesh Ramachandran, Daniel Cossa, Joël Knoery, Nicolas Marusczak, Michelle Nerentorp, and Claus Norstrom. Atmospheric mercury concentrations observed at ground-based monitoring sites globally distributed in the framework of the GMOS network. *Atmospheric Chemistry and Physics*, 16(18):11915–11935, September 2016. Publisher: Copernicus GmbH.

[20] David C. Evers, Susan Egan Keane, Niladri Basu, and David Buck. Evaluating the effectiveness of the Minamata Convention on Mercury: Principles and recommendations for next steps. *Science of The Total Environment*, 569-570:888–903, November 2016.

[21] M. S. Gustin, H. M. Amos, J. Huang, M. B. Miller, and K. Heidecorn. Measuring and modeling mercury in the atmosphere: a critical review. *Atmospheric Chemistry and Physics*, 15(10):5697–5713, 2015. Num Pages: 5697-5713 Place: Katlenburg-Lindau, Germany Publisher: Copernicus GmbH.

[22] Hannah M. Horowitz, Daniel J. Jacob, Yanxu Zhang, Theodore S. Dibble, Franz Slemr, Helen M. Amos, Johan A. Schmidt, Elizabeth S. Corbitt, Eloïse A. Marais, and Elsie M. Sunderland. A new mechanism for atmospheric mercury redox chemistry: implications

for the global mercury budget. *Atmospheric Chemistry and Physics*, 17(10):6353–6371, May 2017. Publisher: Copernicus GmbH.

[23] Viral Shah, Daniel J. Jacob, Colin P. Thackray, Xuan Wang, Elsie M. Sunderland, Theodore S. Dibble, Alfonso Saiz-Lopez, Ivan Černušák, Vladimir Kellö, Pedro J. Castro, Rongrong Wu, and Chuji Wang. Improved Mechanistic Model of the Atmospheric Redox Chemistry of Mercury. *Environmental Science & Technology*, 55(21):14445–14456, November 2021. Publisher: American Chemical Society.

[24] Steve Lindberg, Russell Bullock, Ralf Ebinghaus, Daniel Engstrom, Xinbin Feng, William Fitzgerald, Nicola Pirrone, Eric Prestbo, and Christian Seigneur. A Synthesis of Progress and Uncertainties in Attributing the Sources of Mercury in Deposition. *AMBIO: A Journal of the Human Environment*, 36(1):19–33, February 2007. Publisher: Royal Swedish Academy of Sciences.

[25] William H. Schroeder and John Munthe. Atmospheric mercury—An overview. *Atmospheric Environment*, 32(5):809–822, March 1998.

[26] Matthew S. Landis, Robert K. Stevens, Frank Schaedlich, and Eric M. Prestbo. Development and Characterization of an Annular Denuder Methodology for the Measurement of Divalent Inorganic Reactive Gaseous Mercury in Ambient Air. *Environmental Science & Technology*, 36(13):3000–3009, July 2002. Publisher: American Chemical Society.

[27] Maria Isabel Quant. *Measuring Gradients in Gaseous Elemental Mercury Using a Passive Air Sampler*. Thesis, June 2021. Accepted: 2021-12-29T05:00:27Z.

[28] Mae Sexauer Gustin, Michael S. Bank, Kevin Bishop, Katlin Bowman, Brian Branfireun, John Chételat, Chris S. Eckley, Chad R. Hammerschmidt, Carl Lamborg, Seth Lyman, Antonio Martínez-Cortizas, Jonas Sommar, Martin Tsz-Ki Tsui, and Tong Zhang. Mercury Biogeochemical Cycling: A Synthesis of Recent Scientific Advances. *The Science of the total environment*, 737:139619, October 2020.

[29] Guy P. Brasseur and Daniel J. Jacob. *Modeling of Atmospheric Chemistry*. Cambridge University Press, Cambridge, 2017.

[30] Antonella Macagnano, Paolo Papa, Joshua Avossa, Viviana Perri, Marcello Marelli, Francesca Sprovieri, Emiliano Zampetti, Fabrizio De Cesare, Andrea Bearzotti, and Nicola Pirrone. Passive Sampling of Gaseous Elemental Mercury Based on a Composite TiO2NP/AuNP Layer. *Nanomaterials*, 8(10):798, October 2018. Number: 10 Publisher: Multidisciplinary Digital Publishing Institute.

[31] Ronald Gelaro, Will McCarty, Max J. Suárez, Ricardo Todling, Andrea Molod, Lawrence Takacs, Cynthia Randles, Anton Darmenov, Michael G. Bosilovich, Rolf Reichle, Krzysztof Wargan, Lawrence Coy, Richard Cullather, Clara Draper, Santha Akella, Virginie Buchard, Austin Conaty, Arlindo da Silva, Wei Gu, Gi-Kong Kim, Randal Koster, Robert Lucchesi, Dagmar Merkova, Jon Eric Nielsen, Gary Partyka, Steven Pawson, William Putman, Michele Rienecker, Siegfried D. Schubert, Meta Sienkiewicz, and Bin Zhao. The Modern-Era Retrospective Analysis for Research and Applications, Version 2 (MERRA-2). *Journal of climate*, Volume 30(Iss 13):5419, June 2017. Publisher: NIH Public Access.

[32] J. A. Schmidt, D. J. Jacob, H. M. Horowitz, L. Hu, T. Sherwen, M. J. Evans, Q. Liang, R. M. Suleiman, D. E. Oram, M. Le Breton, C. J. Percival, S. Wang, B. Dix, and R. Volkamer. Modeling the observed tropospheric BrO background: Importance of multiphase chemistry and implications for ozone, OH, and mercury. *Journal of Geophysical Research: Atmospheres*, 121(19):11,819–11,835, 2016. _eprint: https://onlinelibrary.wiley.com/doi/pdf/10.1002/2015JD024229.

[33] F. Steenhuisen and S. J. Wilson. Development and application of an updated geospatial distribution model for gridding 2015 global mercury emissions. *Atmospheric Environment*, 211:138–150, August 2019.

[34] Alkuin Maximilian Koenig, Olivier Magand, Paolo Laj, Marcos Andrade, Isabel Moreno, Fernando Velarde, Grover Salvatierra, René Gutierrez, Luis Blacutt, Diego Aliaga, Thomas Reichler, Karine Sellegri, Olivier Laurent, Michel Ramonet, and Aurélien Dommergue. Seasonal patterns of atmospheric mercury in tropical South America as inferred by a continuous total gaseous mercury record at Chacaltaya station (5240 m) in Bolivia. *Atmospheric Chemistry and Physics*, 21(5):3447–3472, March 2021.

[35] Aryeh Feinberg, Thandolwethu Dlamini, Martin Jiskra, Viral Shah, and Noelle E. Selin. Evaluating atmospheric mercury (Hg) uptake by vegetation in a chemistry-transport model. *Environmental Science: Processes & Impacts*, page 10.1039.D2EM00032F, 2022.

[36] J.D. O'Neill and Kevin H Telmer. Estimating Mercury Use and Documenting Practices in Artisanal and Small-scale Gold Mining (ASGM) - Methods and Tools Version 1.0. 2017.

[37] Artisanal Gold Council. Reporte de Inventario en la MAPE en Peru // Inventory Report for the ASGM sector in Peru. Technical report, 2017.

[38] David G. Streets, Hannah M. Horowitz, Zifeng Lu, Leonard Levin, Colin P. Thackray, and Elsie M. Sunderland. Global and regional trends in mercury emissions and concentrations, 2010–2015. *Atmospheric Environment*, 201:417–427, March 2019.

[39] Jules Sadefo Kamdem. A nice estimation of Gini index and power Pen's parade. *Economic Modelling*, 29(4):1299–1304, July 2012.

[40] Marilena Muntean, Greet Janssens-Maenhout, Shaojie Song, Amanda Giang, Noelle E. Selin, Hui Zhong, Yu Zhao, Jos G. J. Olivier, Diego Guizzardi, Monica Crippa, Edwin Schaaf, and Frank Dentener. Evaluating EDGARv4.tox2 speciated mercury emissions ex-post scenarios and their impacts on modelled global and regional wet deposition patterns. *Atmospheric Environment*, 184:56–68, July 2018.

[41] United Nations Environment Programme. Estimating Mercury Use and Documenting Practices in Artisanal and Small-scale Gold Mining (ASGM) - Methods and Tools Version 1.0. 2017.

[42] P. Bousquet, P. Peylin, P. Ciais, M. Ramonet, and P. Monfray. Inverse modeling of annual atmospheric CO2 sources and sinks: 2. Sensitivity study. *Journal of Geophysical Research: Atmospheres*, 104(D21):26179–26193, 1999. _eprint: https://onlinelibrary.wiley.com/doi/pdf/10.1029/1999JD900341.

[43] M. Kopacz, D. J. Jacob, J. A. Fisher, J. A. Logan, L. Zhang, I. A. Megretskaia, R. M. Yantosca, K. Singh, D. K. Henze, J. P. Burrows, M. Buchwitz, I. Khlystova, W. W. McMillan, J. C. Gille, D. P. Edwards, A. Eldering, V. Thouret, and P. Nedelec. Global estimates of CO sources with high resolution by adjoint inversion of multiple satellite datasets (MOPITT, AIRS, SCIAMACHY, TES). *Atmospheric Chemistry and Physics*, 10(3):855–876, February 2010. Publisher: Copernicus GmbH.

[44] S. Song, N. E. Selin, A. L. Soerensen, H. Angot, R. Artz, S. Brooks, E.-G. Brunke, G. Conley, A. Dommergue, R. Ebinghaus, T. M. Holsen, D. A. Jaffe, S. Kang, P. Kelley, W. T. Luke, O. Magand, K. Marumoto, K. A. Pfaffhuber, X. Ren, G.-R. Sheu, F. Slemr, T. Warneke, A. Weigelt, P. Weiss-Penzias, D. C. Wip, and Q. Zhang. Top-down constraints on atmospheric mercury emissions and implications for global biogeochemical cycling. *Atmospheric Chemistry and Physics*, 15(12):7103–7125, June 2015. Publisher: Copernicus GmbH.

[45] Basil Denzler, Christian Bogdal, Stephan Henne, Daniel Obrist, Martin Steinbacher, and Konrad Hungerbühler. Inversion Approach to Validate Mercury Emissions Based on Background Air Monitoring at the High Altitude Research Station Jungfraujoch (3580 m). *Environmental Science & Technology*, 51(5):2846–2853, March 2017. Publisher: American Chemical Society.

[46] David W. Hogg and Daniel Foreman-Mackey. Data analysis recipes: Using Markov Chain Monte Carlo. *The Astrophysical Journal Supplement Series*, 236(1):11, May 2018. arXiv:1710.06068 [astro-ph, physics:physics, stat].

[47] Lin X Hu X. Ding W, Chen H. Dynamic Brow Restoration Using a Soft Tissue Expander in Adult Patients With Arteriovenous Malformation. January 2020.

[48] M. Rigby, S. Park, T. Saito, L. M. Western, A. L. Redington, X. Fang, S. Henne, A. J. Manning, R. G. Prinn, G. S. Dutton, P. J. Fraser, A. L. Ganesan, B. D. Hall, C. M. Harth, J. Kim, K.-R. Kim, P. B. Krummel, T. Lee, S. Li, Q. Liang, M. F. Lunt, S. A. Montzka, J. Mühle, S. O'Doherty, M.-K. Park, S. Reimann, P. K. Salameh, P. Simmonds, R. L. Tunnicliffe, R. F. Weiss, Y. Yokouchi, and D. Young. Increase in CFC-11 emissions from eastern China based on atmospheric observations. *Nature*, 569(7757):546–550, May 2019. Number: 7757 Publisher: Nature Publishing Group.

[49] Lindsey Konkel. A Safer Gold Rush? Curbing Mercury Pollution in Artisanal and Small-Scale Gold Mining. *Environmental Health Perspectives*, 127(11):112001. Publisher: Environmental Health Perspectives.

[50] Gregory Giuliani, Marion Planque, Antonio Benvenuti, Thomas Piller, Wadood Moomen, and Pierre Lacroix. Technical Guidance Document. page 92, 2022.